Bachelorarbeit
Zur Erlangung des akademischen Grades Bachelor of Science (B.Sc.)

Elastic and lattice-dynamical properties of titanium-based compounds

eingereicht von: Peter Weber

Gutachter/innen: PD Dr. Pasquale Pavone
Prof. Claudia Draxl

Eingereicht am Institut für Physik der Humboldt-Universität zu Berlin am:
11. Februar 2019

Abstract

Titanium is the basic element of a variety of compounds with very different electronic, mechanical, and thermal properties. While, for instance, the rocksalt crystals TiC and TiN are well known for their hardness, allotropes of TiO_2 show much softer elastic behaviour. In this work we present the results of an *ab-initio* investigation of the elastic and lattice-dynamical properties of these compounds under pressure. The elastic-constant tensor is calculated up to the third order. Pressure effects on the lattice-dynamical properties of these compounds are evaluated in terms of the mode Grüneisen parameter at the Brillouin zone center. The calculations are performed using density-functional theory as implemented in the full-potential all-electron software package **`exciting`** [1]. Linear and nonlinear elastic constants are obtained using the **`ElaStic`** tool [2]. The **`ElaStic`** tool is extended to include the calculation of the third-order elastic constants for the tetragonal TI structures.

Contents

1. Introduction

In this work, we focus our attention on four different titanium-based compounds. Two of them, titanium carbide (TiC) and titanium nitride (TiN), crystallize in a rock-salt structure (see Figure 1.1a). They are very well known for their hardness as well as for their high chemical and thermal stability [3]. Both materials are widely used as coating for all sorts of tools [4]. Titanium dioxide (TiO_2) has many different phases. The three most stable ones are rutile (Figure 1.1b), anatase (Figure 1.1c), and brookite. Rutile and antase are characterized by a small number of atoms (6) in the primitive unit cell. TiO_2 is mostly known for its usage in sunscreens. Other usages of TiO_2 are, *e.g.*, in cement as a sterilizer or as coating for self-cleaning classes [5].

Because of the large usage of these materials at different temperatures and pressures, the knowledge of their behavior under extreme conditions is crucial. The response of materials to external (large) solicitations can be described by several material specific values. The goal of this work is the theoretical first-principles determination of some of these values. In particular, we focus on the elastic constants up to the third-order, which gives us a measure of how materials behave under stress. For this set of titanium compounds, we also investigate the phonon frequencies at the center of the Brillouin zone and their variation with the volume. These basic lattice-dynamical properties are relevant for the characterization of the thermal behavior of these compounds.

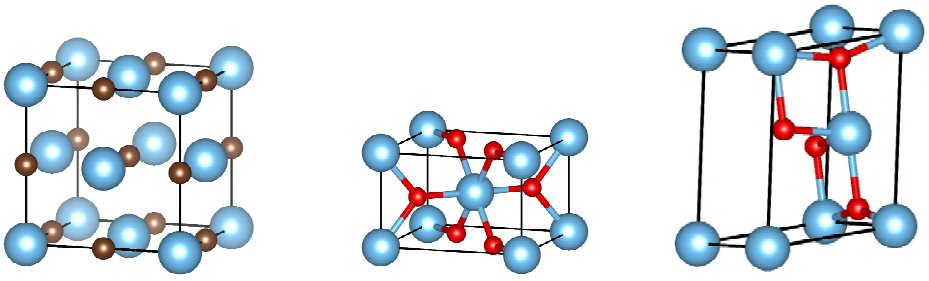

(a) rock salt (b) rutile (c) anatase

Figure 1.1: The crystal structure of rocksalt (a), rutile (b), and anatase (c) systems. Titanium atoms are represented blue, the carbon/nitrogen atoms are brown, and the oxygen atoms are depicted in red.

All calculations presented in this work are based on density-functional theory (DFT). The methodology of DFT as implemented in the software package **exciting** [1] allows for the direct calculation of the total energy and the phonon frequencies of a crystal. In addition to that, the **ElaStic** toolkit [2] is used for obtaining linear and nonlinear elastic constants.

2. Theoretical background

In this chapter, we give a basic theoretical description of the physical properties investigated in this work. At first, we take a look at the theory of elasticity, followed by lattice dynamics. Because both properties are related to changes in the total energy of a crystal, we then look on how to calculate this energy quantum-mechanically. This requires a short description of the density-functional theory (DFT). The last part of this chapter deals with the computational implementation of DFT in the software package **exciting** [1] and with the post-processing tool **ElaStic** [2].

2.1 Elasticity

In the next two sections, we give a short introduction of the mechanical properties of solid materials. A in-depth discussion can be found in standard textbooks [6–9]. In the ideal structure of a crystal its atoms are in an equilibrium state. This means that the summation of all forces acting on them is zero. If we now apply an external force which deforms the crystal, a stress situation is obtained. Atoms move to a new equilibrium position because the internal forces try to compensate the external one. In a macroscopic view, this leads to a deformation of the body. It should be noted that elastic processes are reversible. This means that if the origin of the stress is removed the material returns to its equilibrium state.

2.1.1 Strain

In the elastic limit, a macroscopic state of deformation can be described by the physical strain tensor:

$$\underline{\underline{\boldsymbol{\epsilon}}} = \begin{pmatrix} \epsilon_{xx} & \epsilon_{xy} & \epsilon_{xz} \\ \epsilon_{yx} & \epsilon_{yy} & \epsilon_{yz} \\ \epsilon_{zx} & \epsilon_{zy} & \epsilon_{zz} \end{pmatrix} = \underline{\underline{\boldsymbol{\epsilon}}}^{\mathrm{T}} \,. \tag{2.1}$$

From now on we use the notation in which vectors in 2 or more dimension are written in boldface font (*e.g.*, $\boldsymbol{x}$) and matrices as bold doubly underlined symbols (*e.g.*, $\underline{\underline{\boldsymbol{\epsilon}}}$).

Using the strain tensor in Eq. (2.1) for calculating the deformed position of one atom initially located at $\boldsymbol{x}$, we obtain

$$\boldsymbol{x}' = \underline{\underline{\boldsymbol{J}}} \cdot \boldsymbol{x} \equiv (\underline{\underline{\mathbb{1}}} + \underline{\underline{\boldsymbol{\epsilon}}}) \cdot \boldsymbol{x} \,, \tag{2.2}$$

where $\underline{\underline{\boldsymbol{J}}}$ is the deformation matrix. Diagonal elements of the physical strain tensor describe deformations along the axes, while mixed elements describe a shearing. In Figure 2.1 we can see some examples of different strains.

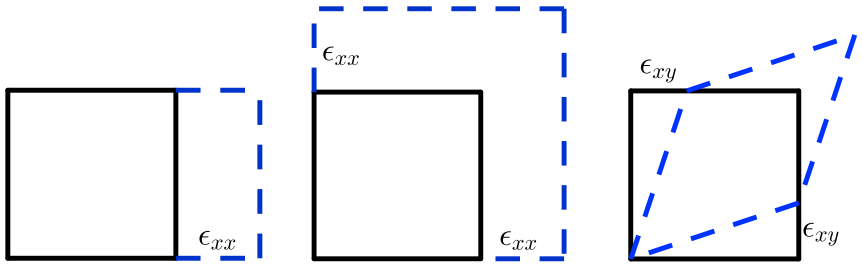

(a) Uniaxial strain (b) Expansion (c) Shear

Figure 2.1: Examples of different strains in a two-dimensional space.

These examples correspond to the following two-dimensional strain tensors:

$$(a)\ \ \underline{\underline{\boldsymbol{\epsilon}}} = \begin{pmatrix} \epsilon_{xx} & 0 \\ 0 & 0 \end{pmatrix} \,; \qquad (b)\ \ \underline{\underline{\boldsymbol{\epsilon}}} = \begin{pmatrix} \epsilon_{xx} & 0 \\ 0 & \epsilon_{xx} \end{pmatrix} \,; \qquad (c)\ \ \underline{\underline{\boldsymbol{\epsilon}}} = \begin{pmatrix} 0 & \epsilon_{xy} \\ \epsilon_{xy} & 0 \end{pmatrix} \,.$$

An alternative definition of the strain is represented by the Lagrangian strain $\underline{\underline{\boldsymbol{\eta}}}$. In contrast to the physical strain, the Lagrangian one is defined by the change of the length of a general vector $\boldsymbol{v}$ under deformation:

$$|\boldsymbol{v}'|^2 - |\boldsymbol{v}|^2 = 2\, \boldsymbol{v} \cdot \underline{\underline{\boldsymbol{\eta}}} \cdot \boldsymbol{v} \,. \tag{2.3}$$

The Lagrangian strain tensor $\underline{\underline{\boldsymbol{\eta}}}$ is thermodynamically invariant, and Brugger [10] has shown that this strain gives the thermodynamically correct third-order elastic constants. The strain $\underline{\underline{\boldsymbol{\eta}}}$ can be related to the physical strain $\underline{\underline{\boldsymbol{\epsilon}}}$ by

$$\underline{\underline{\boldsymbol{\eta}}} = \underline{\underline{\boldsymbol{\epsilon}}} + \frac{1}{2}\, \underline{\underline{\boldsymbol{\epsilon}}}^2 \,. \tag{2.4}$$

We notice that $\boldsymbol{\eta} \cong \boldsymbol{\epsilon}$ at small strains. Like the physical strain, also the Lagrangian one is symmetrical. Due to this fact, we can write both in the Voigt notation:

$$\begin{aligned} &\eta_{11} \to \eta_1 && \eta_{22} \to \eta_2 && \eta_{33} \to \eta_3 \\ &\eta_{23} \to 2\eta_4 && \eta_{13} \to 2\eta_5 && \eta_{12} \to 2\eta_6 \,. \end{aligned} \tag{2.5}$$

This notation turns the 3×3-matrix $\underline{\underline{\boldsymbol{\eta}}}$ into a 6-dimensional vector $\boldsymbol{\eta}$.

2.1.2 Elastic constants

Performing a Taylor expansion of the energy of the crystal in $\boldsymbol{\eta}$ around the initial equilibrium state, we get:

$$E(\boldsymbol{\eta}) = E(0) + \sum_{i=1}^{6} \left.\frac{\partial E}{\partial \eta_i}\right|_0 \eta_i + \frac{1}{2}\sum_{i=1}^{6}\sum_{j=1}^{6} \left.\frac{\partial^2 E}{\partial \eta_i \partial \eta_j}\right|_0 \eta_i\,\eta_j + \frac{1}{6}\sum_{i=1}^{6}\sum_{j=1}^{6}\sum_{k=1}^{6} \left.\frac{\partial^3 E}{\partial \eta_i \partial \eta_j \partial \eta_k}\right|_0 \eta_i\,\eta_j\,\eta_k + \mathcal{O}(\boldsymbol{\eta}^4)\,. \tag{2.6}$$

The first summand on the r.h.s. of this equation is the equilibrium energy of the initial state. The second is related to the stress $\boldsymbol{\sigma}_0$ acting on the system in the initial configuration:

$$\boldsymbol{\sigma}_0 = \frac{1}{V}\left.\frac{\partial E(\boldsymbol{\eta})}{\partial \boldsymbol{\eta}}\right|_0\,. \tag{2.7}$$

This stress is zero for the equilibrium state. The higher-order derivatives of the energy are related to the elastic constants. The second-order derivatives in Eq. (2.6) leads to the second-order elastic constants (SOECs):

$$c_{ij} = \frac{1}{V}\left.\frac{\partial^2 E}{\partial \eta_i\,\partial \eta_j}\right|_0\,, \tag{2.8}$$

where symmetrical $\underline{\underline{\boldsymbol{c}}}$ is a 6×6 matrix. Similarly, we get the third-order elastic constants (TOECs):

$$c^{(3)}_{ijk} = \frac{1}{V}\left.\frac{\partial^3 E}{\partial \eta_i\,\partial \eta_j\,\partial \eta_k}\right|_0\,. \tag{2.9}$$

With the elastic constants, the expansion in Eq. (2.6) can be written for the energy in a unit cell with the volume $V = \Omega$ as

$$E(\boldsymbol{\eta}) = E_0 + \frac{\Omega}{2}\sum_{i,j=1}^{6} c_{ij}\,\eta_i\,\eta_j + \frac{\Omega}{6}\sum_{i,j,k=1}^{6} c^{(3)}_{ijk}\,\eta_i\,\eta_j\,\eta_k + \mathcal{O}(\boldsymbol{\eta}^4)\,. \tag{2.10}$$

Terms in Eq. (2.10) up the second-order describe the linear elasticity. Higher-order contributions are denominated non-linear terms.

2.2 Lattice dynamics

In the previous sections, we discussed a static deformation of a crystal. Now, we look at dynamic deformations at very small scales. This corresponds to atomic vibrations, which are important to many material properties like, *e.g.*, thermal expansion, optical absorption, and structural phase transitions. Collective atomic vibrations can be interpreted in terms of quasi-particles which we call phonons. In this section, we discuss how we can obtain the frequencies of such phonons as well as their dependence on the unit-cell volume, as represented by the mode Grüneisen parameters.

2.2.1 Phonon frequencies

If we displace atoms from their equilibrium position without an external force, they try to resume to their equilibrium positions. Assuming no damping, this leads to harmonic-like oscillations around their equilibrium positions. In this section, we show how the frequencies of these oscillations can be formally obtained.

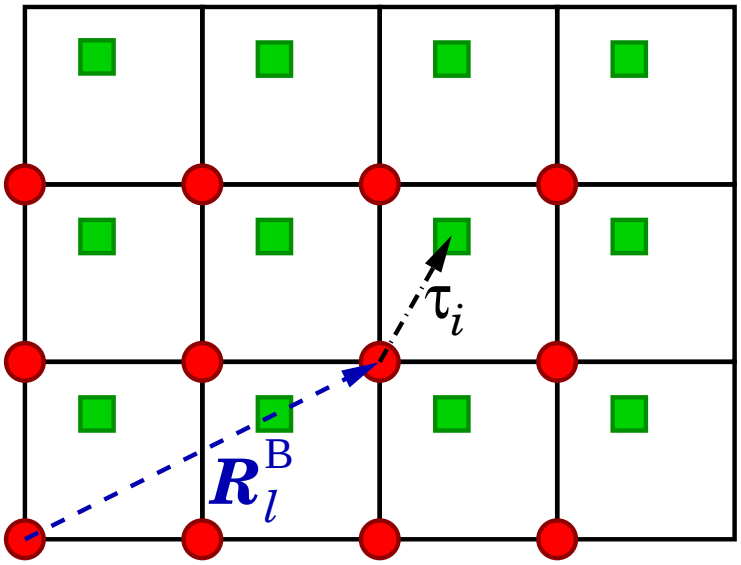

Figure 2.2: Schematic representation of a two-dimensional crystal with a basis of two atoms in the unit cell.

We can define the equilibrium position of an atom in a crystal structure (see Figure 2.2) by

$$\boldsymbol{R}_{li}^0 = \boldsymbol{R}_l^{\mathrm{B}} + \boldsymbol{\tau}_i \,, \tag{2.11}$$

where $\boldsymbol{R}_l^{\mathrm{B}}$ is the Bravais lattice vector, $\boldsymbol{\tau}_i$ the equilibrium position of the i-th atom in the basis. The time-dependent displaced position of the atom can be written as

$$\boldsymbol{R}_{li}(t) = \boldsymbol{R}_{li}^0 + \boldsymbol{S}_{li}(t) \,, \tag{2.12}$$

where $\boldsymbol{S}_{li}(t)$ is the displacement at time t. For a further simplification we join the index i and the Cartesian index together in a new index μ. Using this notation, in $R_{l\mu}(t)$ only the displacement component $S_{l\mu}(t)$ is time dependent.

In the Born-Oppenheimer approximation [11], the classical Euler-Lagrange equations of motion for the nuclei (atoms) read:

$$M_\mu \, \ddot{S}_{l\mu} = -\frac{\partial U}{\partial S_{l\mu}} \,, \tag{2.13}$$

where M_μ is the mass of atom i. To solve these equations, we need the potential

$U(S)$ as a function of the atomic displacements. Expanding $U(S)$ in terms of small displacements one gets:

$$U(S) = E_0 + \sum_{l\mu} \left.\frac{\partial U}{\partial S_{l\mu}}\right|_0 S_{l\mu} + \frac{1}{2}\sum_{l\mu}\sum_{l'\mu'} \left.\frac{\partial^2 U}{\partial S_{l\mu}\partial S_{l'\mu'}}\right|_0 S_{l\mu}\, S_{l'\mu'} + \mathcal{O}(S^3)\,. \tag{2.14}$$

Similarly to Eq. (2.6), the second summand in Eq. (2.14) is zero because forces vanish at the equilibrium. Equation (2.14) can be written in the harmonic approximation, neglecting $\mathcal{O}(S^3)$ terms, as

$$U_{\mathrm{harm}}(S) = E_0 + \frac{1}{2}\sum_{l\mu}\sum_{l'\mu'} \Phi^{l\mu}_{l'\mu'}\, S_{l\mu}\, S_{l'\mu'}\,, \tag{2.15}$$

where $\Phi^{l\mu}_{l'\mu'}$ are the interatomic force constants at equilibrium. Using Eqs. (2.13) and (2.15), we obtain the equations of motion in the form

$$M_\mu\, \ddot{S}_{l\mu}(t) = -\sum_{l'\mu'} \Phi^{l\mu}_{l'\mu'}\, S_{l'\mu'}(t)\,. \tag{2.16}$$

To solve these differential equations, the periodicity of the crystal suggests the following Bloch-like *ansatz*:

$$S_{l\mu}(t) = \frac{1}{\sqrt{M_\mu}}\, w_\mu(\boldsymbol{q})\, e^{i\,(\boldsymbol{q}\cdot\boldsymbol{R}^{\mathrm{B}}_l - \omega\, t)}\,. \tag{2.17}$$

Inserting the *ansatz* (2.17) in Eq. (2.16), leads to the eigenvalue equation

$$\underline{\underline{\boldsymbol{D}}}(\boldsymbol{q})\, \boldsymbol{w}(\boldsymbol{q}) = \omega^2(\boldsymbol{q})\, \boldsymbol{w}(\boldsymbol{q})\,, \tag{2.18}$$

where $D_{\mu\mu'}$ is the dynamical matrix

$$D_{\mu\mu'}(\boldsymbol{q}) = \frac{1}{\sqrt{M_\mu\, M_{\mu'}}} \sum_l \Phi^{0\mu}_{l\mu'}\, e^{i\,\boldsymbol{q}\cdot\boldsymbol{R}^{\mathrm{B}}_l}\,. \tag{2.19}$$

Solving the eigenvalue problem in Eq. (2.18), we obtain the phonon frequencies $\omega(\boldsymbol{q})$.

2.2.2 Grüneisen parameters

The dynamical matrix $\underline{\underline{\boldsymbol{D}}}$ defined in the previous section is evaluated at the equilibrium positions $\boldsymbol{R}^0_l$. If the crystal is strained, however, the atomic positions change, too. Therefore, the interatomic force constants, dynamical matrix, and phonon frequencies of the strained crystal have to be evaluated in the new positions. This leads to a change in the elements of the dynamical matrix and to a shift of the phonon frequencies. These changes from the equilibrium state can be measured by the mode Grüneisen parameters, defined as:

$$\gamma_\nu(\boldsymbol{q},\epsilon_j) = -\frac{1}{\omega_\nu(\boldsymbol{q};0)} \left(\frac{\omega_\nu(\boldsymbol{q};\epsilon_j)}{\partial\epsilon_j}\right)_{\epsilon_j=0}\,. \tag{2.20}$$

Notice that Eq. (2.20) depends explicitly on the strain component ϵ_j. The mode Grüneisen parameter, $\gamma_\nu(\boldsymbol{q},\epsilon_j)$, is a measure of the change of the phonon frequency $\omega_\nu(\boldsymbol{q})$ under a small deformation of the geometry of the unit cell caused by the strain ϵ_j. In Eq. (2.20) the index ν refers to the phonon mode, while the index j refers to the strain in the Voigt notation. For a small hydrostatic-pressure deformation ($\epsilon_j = \epsilon$ for $j = 1, 2, 3$ and $\epsilon_j = 0$ for $j = 4, 5, 6$), we can express Eq. (2.20) as

$$\left(\frac{\Delta\omega_\nu(\boldsymbol{q})}{\omega_\nu(\boldsymbol{q})}\right) = -\gamma_\nu(\boldsymbol{q};\epsilon)\,\frac{\Delta a_j}{a_j} = -\gamma_\nu(\boldsymbol{q};\epsilon)\,\epsilon\,, \tag{2.21}$$

where a_j are the lengths of the 3 vectors which identify the unit cell of the crystal. Using Eq. (2.21), we get the dependence of the mode Grüneisen parameter for cubic systems (where $a_1 = a_2 = a_3$) on the volume of the unit cell Ω:

$$\gamma_\nu(\boldsymbol{q},\Omega) = -\frac{\Omega}{\omega_\nu(\boldsymbol{q})}\left(\frac{\partial\omega_\nu(\boldsymbol{q})}{\partial\Omega}\right)\,. \tag{2.22}$$

For tetragonal systems, where $a = a_1 = a_2 \neq a_3 = c$, we get:

$$\gamma_\nu(\boldsymbol{q},\Omega) = -2\left(\frac{\partial\ln\omega_\nu(\boldsymbol{q};a)}{\partial\ln a}\right)\left(\frac{\mathrm{d}\ln a}{\mathrm{d}\ln\Omega}\right) - \left(\frac{\partial\ln\omega_\nu(\boldsymbol{q};c)}{\partial\ln c}\right)\left(\frac{\mathrm{d}\ln c}{\mathrm{d}\ln\Omega}\right)\,. \tag{2.23}$$

2.3 Total energy from quantum mechanics

To calculate the energy $\mathcal{E}_{\mathrm{tot}}$ of a system of electrons and nuclei using quantum mechanics, we have to solve the Schrödinger equation:

$$\hat{H}\,\Psi(r,R) = \mathcal{E}_{\mathrm{tot}}\,\Psi(r,R)\,, \tag{2.24}$$

where $r = \{\boldsymbol{r}_i;\, i = 1,..,N\}$, $R = \{\boldsymbol{R}_I;\, I = 1,..,N_n\}$, and $\Psi(r,R)$ is the wavefunction of the total system of both nuclei and electrons. $\hat{H}$ is the Hamiltonian of the total system. It contains the kinetic-energy operators for the electrons and nuclei ($\hat{T}_e$ and $\hat{T}_n$) as well as the Coulomb potentials ($\hat{V}_{nn}$, $\hat{V}_{ee}$, and $\hat{V}_{ne}$) acting between them.

Using the Born-Oppenheimer (BO) approximation [11], the ground-state wavefunction can be written as

$$\Psi_{\mathrm{GS}}(r,R) = \varphi_0(r,R)\,\chi_0(R)\,, \tag{2.25}$$

in terms of the electronic, $\varphi_0(r,R)$, and nuclear, $\chi_0(R)$, wavefunctions. Using Eqs. (2.24) and (2.25) we reach an effective equation which depends only on the nuclear coordinates:

$$\hat{H}_{\mathrm{BO}}\,\chi_0(R) = \left[\hat{T}_n + \hat{V}_{nn} + E_0(R)\right]\chi_0(R) = \mathcal{E}_{\mathrm{tot}}^{\mathrm{BO}}\,\chi_0(R)\,, \tag{2.26}$$

where $\hat{T}_n$ is the kinetic energy operator of the nuclei and $\hat{V}_{nn}$ the nuclei-nuclei potential (a simple Coulomb potential). $E_0(R)$ is the ground-state energy of the electron system with the nuclear positions in configuration R. H_{BO} can be interpreted as a nuclear Hamiltonian with an effective potential

$$U(R) = \hat{V}_{nn}(R) + E_0(R) \,. \tag{2.27}$$

The ground-state energy $E_0(R)$ of the electron system is obtained solving the electronic equation:

$$\hat{H}_e \, \varphi_0(r;R) = \left[\hat{T} + \hat{W} + \hat{V}(R)\right] \varphi_0(r;R) = E_0(R) \, \varphi_0(r;R) \,, \tag{2.28}$$

where $\hat{T}$ is the kinetic-energy operator for the electrons, $\hat{W}$ the potential between electrons, and $\hat{V}$ the external nuclear potential acting on the electrons.

2.4 Density-functional theory

To calculate the phonon frequencies and the elastic constants as shown in the previous sections, we need the effective nuclear potential defined in Eq. (2.27). While $\hat{V}_{nn}$ is just the Coulomb potential between the nuclei, E_0 can not be calculated so easily. The method we use to calculate E_0 is density-functional theory (DFT) which is shortly discussed in this section.

The foundation of DFT is based on the Hohenberg-Kohn theorem [12], which states that every external potential $\hat{V}$ has a one-to-one correspondence to its ground-state density $n_{\mathrm{GS}}(\boldsymbol{r})$. A consequence of this theorem is also that every observable can be expressed as a functional of the ground-state density. Kohn and Sham (KS) developed an approach which allows for a relatively easy calculation of both ground-state density and energy [13]. This approach represents the basis for a large amount of calculations of materials properties.

Following Kohn and Sham, the ground-state energy functional is written as

$$\begin{aligned} E_{\mathrm{GS}}[n] &= <\varphi_{\mathrm{GS}}[n]|\hat{T} + \hat{W} + \hat{V}|\varphi_{\mathrm{GS}}[n]> \\ &= T_0[n] + E_{\mathrm{H}}[n] + E_{\mathrm{ext}}[n] + E_{\mathrm{xc}}[n] \,, \end{aligned} \tag{2.29}$$

where $T_0[n]$ is the universal kinetic-energy functional of a non-interacting electron system, $E_{\mathrm{H}}[n]$ the Hartree energy functional, $E_{\mathrm{ext}}[n]$ is the energy functional corresponding to the external potential $\hat{V}$, and $E_{\mathrm{xc}}[n]$ is the (unknown) exchange-correlation functional. The Hohenberg-Kohn theorem establishes that if $E_{\mathrm{GS}}[n]$ exists, then $E_{\mathrm{GS}}[n] \geq E_{\mathrm{GS}}[n_{\mathrm{GS}}]$. This means that we can obtain the ground-state

density n_{GS} by minimizing E_{GS}, which leads to the equation

$$\frac{\delta T_0[n]}{\delta n(\boldsymbol{r})} + v_{\mathrm{KS}}(\boldsymbol{r},[n]) = \mu\,, \tag{2.30}$$

where μ is the chemical potential [14] and the Kohn-Sham (KS) potential is defined by

$$\begin{aligned} v_{\mathrm{KS}}(\boldsymbol{r},[n]) &= \frac{\delta E_{\mathrm{H}}[n]}{\delta n(\boldsymbol{r})} + \frac{\delta E_{\mathrm{ext}}[n]}{\delta n(\boldsymbol{r})} + \frac{\delta E_{\mathrm{xc}}[n]}{\delta n(\boldsymbol{r})} \\ &= v_{\mathrm{H}}(\boldsymbol{r},[n]) + v(\boldsymbol{r}) + v_{\mathrm{xc}}(\boldsymbol{r},[n])\,. \end{aligned} \tag{2.31}$$

Equation (2.30) holds for the interacting electron system, however, it is identical to the one obtained for a non-interacting electron system ($\hat{W} = 0$) in the external potential v_{KS} and with the same ground-state density n_{GS}. Performing the explicit minimization for the non interacting system, we achieve the single-particle Kohn-Sham equations:

$$\hat{h}_{\mathrm{KS}}\, u_i(\boldsymbol{r}) \equiv \left[-\frac{\nabla^2}{2} + v_{\mathrm{KS}}(\boldsymbol{r},[n])\right] u_i(\boldsymbol{r}) = \varepsilon_i\, u_i(\boldsymbol{r})\,. \tag{2.32}$$

After solving the KS equations, the density n_{GS} can be easily calculated as

$$n_{\mathrm{GS}}(\boldsymbol{r}) = \sum_{i=1}^{N} |u_i(\boldsymbol{r})|^2\,, \tag{2.33}$$

where N is the number of electrons in the system. Due to the fact that v_{KS} depends on n_{GS}, the KS equations must be solved self-consistently, as shown in Figure 2.3.

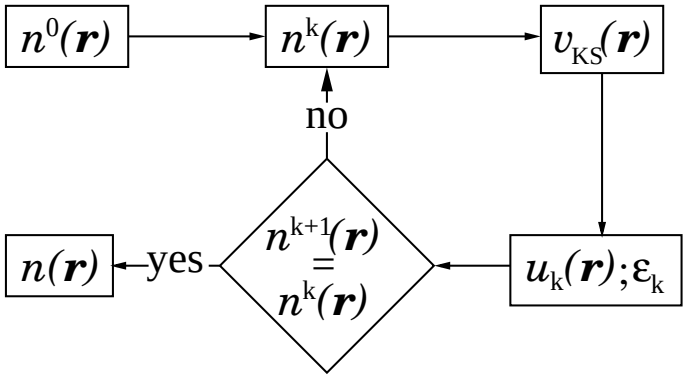

Figure 2.3: Schematic representation of the self-consistent cycle for the ground-state density as solution of the Kohn-Sham equations.

It is important to mention that, in Eq. (2.32), neither ε_i nor $u_i(\boldsymbol{r})$ have a physical meaning, nevertheless, we get the correct ground-state density using the KS equations as long as we assume, that we use the exact E_{xc}.

The Kohn-Sham equations by themselves are not an approximation. However, we have to acknowledge, that the exchange-correlation potential v_{xc} in Eq. (2.31) is

not known. Thus, we have to do an approximation at this point. There are many different methods to approximate this potential [15]. Some of them are more accurate but in return more expensive in the computational effort. An "easy" approximation is the local-density approximation (`LDA`), which yields the exchange-correlation energy $E_{\mathrm{xc}}[n]$ using results for the homogeneous electron gas, and therefore only depends on $n(\boldsymbol{r})$. Another class of exchange-correlation functionals is given by the generalized gradient approximations (`GGA`). Contrary to `LDA`, these functionals are also using the gradient of the density $\nabla n(\boldsymbol{r})$.

2.5 Solution of the Kohn-Sham equations

The self-consistent solution of the Kohn-Sham equations requires the use of a numerical approach. To keep the computational cost low and, at the same time, to efficiently represent electron wavefunctions, we use an expansion of the solution of Eq. (2.32) in terms of a finite basis set

$$u_i(\boldsymbol{r}) = \sum_{j=1}^{j_{\max}} C_i^j \, \phi_i^j(\boldsymbol{r}). \tag{2.34}$$

Then, the KS equations can be written, for a given quantum number i, as a generalized eigenvalue problem:

$$\left(\underline{\underline{\boldsymbol{H}}} - \varepsilon_i \, \underline{\underline{\boldsymbol{O}}}\right) \cdot \boldsymbol{C} = 0 \, , \tag{2.35}$$

where $\underline{\underline{\boldsymbol{H}}}$ is the KS-hamiltonian matrix with elements

$$H_{\alpha\beta} = \langle \phi_i^\alpha | \, \hat{h}_{\mathrm{KS}} \left| \phi_i^\beta \right\rangle \, , \tag{2.36}$$

$\underline{\underline{\boldsymbol{O}}}$ is the overlap matrix defined by

$$O_{\alpha\beta} = \langle \phi_i^\alpha | \, \phi_i^\beta \rangle \, , \tag{2.37}$$

and $\boldsymbol{C}$ is the eigenvector consisting of the coefficients C_i^j. For a periodic crystal the quantum number i can be rewritten as $i \to (i, \boldsymbol{k})$, where the index i is the band index and $\boldsymbol{k}$ is the wave vector.

2.6 The software package `exciting`

In order to calculate the total energy of a crystal, we use the full-potential all-electron code **`exciting`** [1]. The flowchart in Figure 2.4 shows how **`exciting`** calculates the ground-state density. First, it starts with an initial guess for the density, *e.g.*, by a superposition of the atomic densities. In a second step, it calculates the core

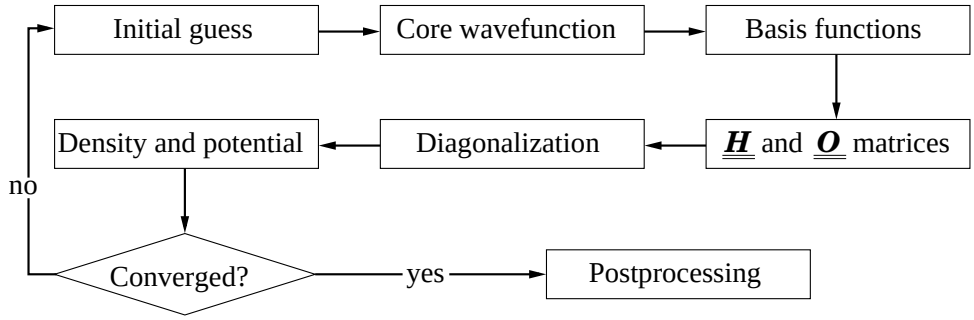

Figure 2.4: Flowchart for the self-consistent solution of the KS equation in the (L)APW+lo basis (variation of figure from Ref. [1]).

wavefunctions which are treated like we would do for free atoms. Then, a basis set representation is introduced, as discussed in the next section. Through setting up the matrices $\underline{\underline{\boldsymbol{H}}}$ and $\underline{\underline{\boldsymbol{O}}}$ in $\boldsymbol{k}$-space and diagonalizing them, we get the new density. If the density is converged, we can start the postprocessing. Otherwise, it starts the cycle again using a mixture of the previously obtained densities.

2.6.1 Basis functions in `exciting`

The **`exciting`** code employed in this work uses the linearized augmented plane waves plus local orbitals as basis set. The idea behind the plane-wave augmentation is to describe the KS wavefunctions for a crystal, $u_{i\boldsymbol{k}}(\boldsymbol{r})$, as a combination of atomic-like functions in a muffin-tin (MT) region near the atoms and plane waves in the remaining interstitial (I) region. The MT region consists of non-overlapping spheres with radius R^{α}_{MT} centered on the atoms at position $\boldsymbol{R}_{\alpha}$. The KS wavefunctions can be written as linear combination of augmented plane waves (APWs):

$$u_{i\,\boldsymbol{k}}(\boldsymbol{r}) = \sum_{\boldsymbol{G}} C^{i\,\boldsymbol{k}}_{\boldsymbol{G}}\, \phi_{\boldsymbol{G}+\boldsymbol{k}}(\boldsymbol{r})\;, \tag{2.38}$$

where $\boldsymbol{G}$ is a reciprocal-lattice vector, and the APWs are given as

$$\phi_{\boldsymbol{G}+\boldsymbol{k}}(\boldsymbol{r}) = \begin{cases} \displaystyle\sum_{lm} A^{\boldsymbol{G}+\boldsymbol{k}}_{lm\alpha}\, X_{l\alpha}(r_{\alpha};\varepsilon_{l\alpha})\, Y_{lm}(\hat{\boldsymbol{r}}_{\alpha}), & r_{\alpha} \le R^{\alpha}_{\mathrm{MT}} \\ \dfrac{1}{\sqrt{\Omega}}\, e^{i(\boldsymbol{G}+\boldsymbol{k})\cdot\boldsymbol{r}}, & \boldsymbol{r} \in I\;, \end{cases} \tag{2.39}$$

where $\boldsymbol{r}_{\alpha} = \boldsymbol{r} - \boldsymbol{R}_{\alpha}$ and $\varepsilon_{l\alpha}$ is an energy parameter approximating the eigenenergies of states with angular momentum l for atom α. The MT part of the APW is built by the spherical harmonics $Y_{ml}(\hat{\boldsymbol{r}}_{\alpha})$, the radial function $X_{l\alpha}(r_{\alpha};\varepsilon_{l\alpha})$, and a coefficient $A^{\boldsymbol{G}+\boldsymbol{k}}_{lm\alpha}$ which makes the APW continuous at the MT boundary. Alternatively, linearized augmented plane waves (LAPW) can be used as basis. In this case, the basis function

inside the MT region is

$$\phi_{\boldsymbol{G}+\boldsymbol{k}}(\boldsymbol{r}) = \sum_{lm} \left[A_{lm\alpha}^{\boldsymbol{G}+\boldsymbol{k}}\, X_{l\alpha}(r_\alpha; \varepsilon_{l\alpha}) + B_{lm\alpha}^{\boldsymbol{G}+\boldsymbol{k}}\, \dot{X}_{l\alpha}(r_\alpha; \varepsilon_{l\alpha}) \right] Y_{lm}(\hat{\boldsymbol{r}}_\alpha)\,, \tag{2.40}$$

where the further constants, $B_{lm\alpha}^{\boldsymbol{G}+\boldsymbol{k}}$, allow for continuity of the derivative of the LAPW at the MT boundary, too.

To improve the description of the KS wavefunctions inside the MT region, "local orbitals" (lo) which are vanishing in the interstitial region are added to the basis functions. Finally, we have:

$$u_{i\boldsymbol{k}}(\boldsymbol{r}) = \sum_{\boldsymbol{G}} C_{\boldsymbol{G}}^{i\boldsymbol{k}}\, \phi_{\boldsymbol{G}+\boldsymbol{k}}(\boldsymbol{r}) + \sum_{\nu} C_{\nu}^{i\boldsymbol{k}}\, \phi_{\nu}^{\mathrm{lo}}(\boldsymbol{r})\,. \tag{2.41}$$

The basis set size is kept finite by considering a finite number of local orbitals and by limiting the allowed values of $\boldsymbol{G}$ with a maximum cut-off value $G_{\max}$. If we reduce the muffin-tin radius R_{MT} we need more plane waves to describe appropriately the wavefunction in the interstitial region. Thus, the proper parameter which gives a measure of the basis set size is the product $R_{\mathrm{MT}}^{\min} G_{\max}$ of the minimum MT radius and the value of $G_{\max}$.

2.7 The `ElaStic` tool

In this work, the elastic constants introduced in Section 2.1.2 are obtained by using the **`ElaStic`** toolkit [2]. Figure 2.5 shows the procedure **`ElaStic`** uses to calculate elastic constants. At first, **`ElaStic`** determines the numbers of deformations needed to achieve all independent components of the elastic tensor. To this purpose, the

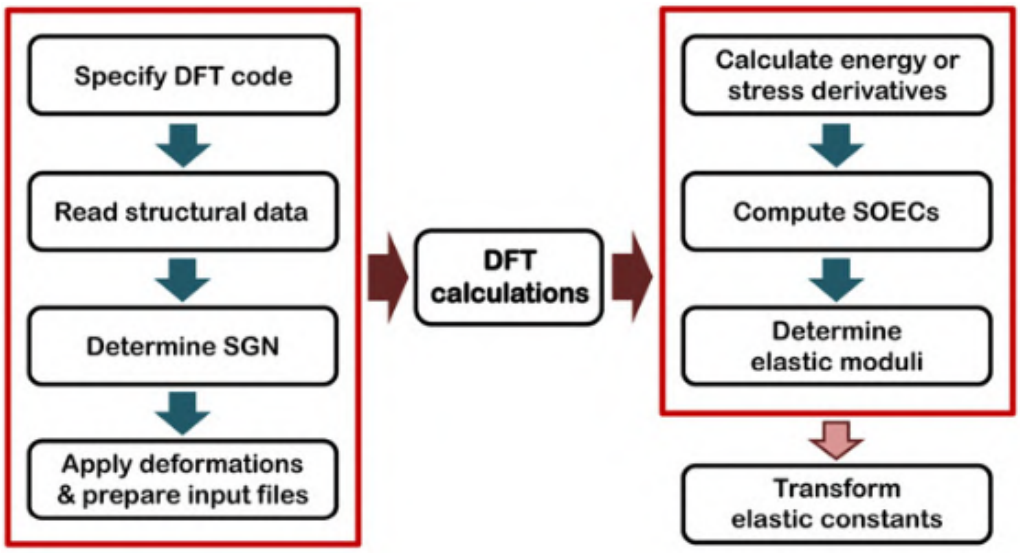

Figure 2.5: Flowchart of the algorithm used in the **`ElaStic`** tool taken from Ref. [2].

tool uses the program **sgroup** [16] to verify the Laue group of the crystal. Then, according to the determined Laue group, different types of deformations are applied to the crystal. Each type of deformation is represented by a strain vector, which has a given expresion in terms of the strain amplitude η. For a certain number of values of $\eta \in [-\eta_{\max}, \eta_{\max}]$ strained structures are obtained. For every structure a DFT calculation is performed using **exciting**. Then, the achieved energy-strain pairs for a given type of deformation are fitted by polynomial functions of degree n:

$$E(\eta) = \sum_{i=0}^{n} A_i \, \eta^i \, , \tag{2.42}$$

where A_i are the fitting coefficients. The fitting procedure is applied to intervals of strain values of increasing size, until all calculated energy-strain pairs are taken into consideration. Correspondingly to every fit, we get a value of the energy derivative of the given order. According to Eq. (2.42), the fit of the second- (third-)order derivative yields the value of $2A_2$ ($6A_3$). These values are plotted as a function of the size of the strain interval (measured by $\eta_{\max}$). Figure 2.6 shows a schematic example for such a plot, where the values of $n = 2, 4$, and 6 are considered.

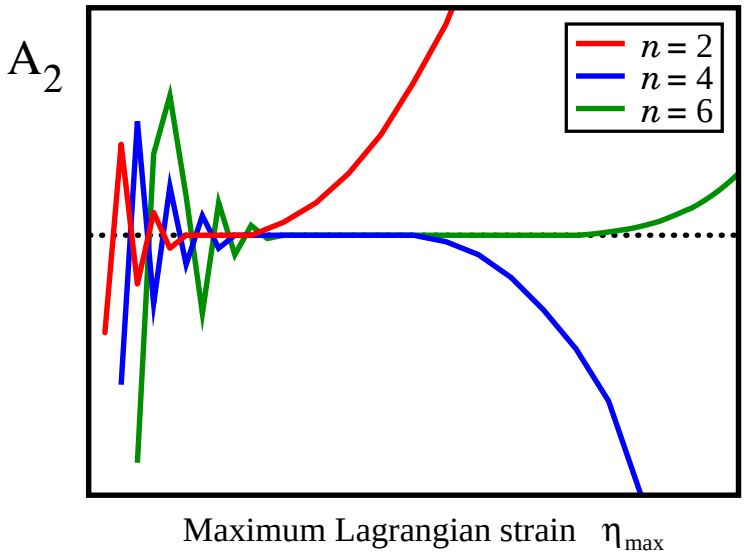

Figure 2.6: Simple scheme of a plot from **ElaStic** for the second-order derivatives. The dotted line represents the "true" unbiased value of A_2 (see text).

As we can see in Figure 2.6, the results for A_2 at low $\eta_{\max}$ are varying a lot. In this region the energy values have only minor differences, therefore, the influence of the numerical noise is larger. This effect is more evident for higher-order polynomial fits. At large values of $\eta_{\max}$, we see that the curve related to a polynominal fit of a given order deviates from the "true" unbiased result, *i.e.*, the value obtained for "infinite"

numerical accuracy of the calculations. Therefore, the best numerical value for A_2 is obtained in the region of intermediate values of $\eta_{\max}$, with the size of this region becoming larger for larger values of n. We note that this region is just the one where the results show a "plateau". The constant A_2 (A_3) is a linear combination of elastic constants. Considering all coefficients A_2 (A_3) for all the deformation types, we get a system of linear equations where the unknowns are the independent components of the elastic tensor. Finally, **`ElaStic`** obtains the elastic constants c_{ij} $\left(c^{(3)}_{ijk}\right)$ by solving this system of linear equations.

3. Results

In this chapter, we show the results of *ab-initio* calculations performed for TiC, TiN, and two allotropes of TiO_2. All results are obtained using the all-electron full-potential code **exciting**. At first, we specify the used functionals and the computational parameters we set in the **exciting** calculations. Then, we investigate the properties of the equilibrium structures. With this pre-requisites, we calculate linear and non-linear elastic constants as well as phonon frequencies and their volume derivatives.

3.1 Computational details

The *ab-initio* methodology based on density-functional theory requires the choice of an approximated exchange-correlation functional. In this work, we use the generalized gradient approximation (GGA), introduced in Section 2.4. In particular, we employ the functional form developed by Perdew, Burke, and Ernzerhof (PBE) [17] for compatibility with other works. Some calculations are also done with the PBEsol functional [18], which is claimed to be the most accurate for solids [19].

Basis functions in the muffin-tin region have to be specified for each used element. In **exciting** this is achieved by using for each element a corresponding "species" file fully characterizing the basis set. For all calculations the same titanium species file is employed. The $1s^2$, $2s^2$, and $2p^6$ states of Ti are treated as core states. For nitrogen, oxygen, and carbon always the 1s state is treated as core state. In addition, several local orbitals are used for all elements. The complete species files can be found in Appendix A.

Furthermore, in **exciting** there is a bunch of parameters whose values determine the quality of the numerical description of the system. To achieve the desired precision of the physical properties that are the target of the calculation, these parameters have to be optimized. To this purpose, we first choose a representative subset of the physical quantities of interest. In our case, they are:

1. The bulk modulus at equilibrium (zero pressure, $p = 0$):

$$B_0 = -\Omega_0 \left(\frac{\partial p}{\partial \Omega} \right)_{p=0}, \tag{3.1}$$

   which is a linear combination of second-order elastic constants (SOECs).

2. The pressure derivative of the bulk modulus B, calculated at zero pressure, $B_0' = (\partial B/\partial p)_{p=0}$. This dimensionless quantity is related to the third-order elastic constants (TOECs).

3. A transverse-optical phonon frequency at the Γ point, $\omega_{\mathrm{TO}}(\Gamma)$, as test case for the lattice-dynamical calculations.

These target properties are calculated for different sets of values of the computational parameters. By increasing the quality of the numerical description, calculations are assumed to be "converged" if the absolute variation of the values of the target properties do not exceed a given (small) quantity, which we define as precision. We fix this precision to 0.1 GPa for B_0, 10^{-2} for B_0', and $1\,\mathrm{cm}^{-1}$ for $\omega_{\mathrm{TO}}(\Gamma)$.

In order to achieve the precision introduced above, the first important parameter needed to be varied is the size of the basis set as expressed by the product $R_{\mathrm{MT}}^{\mathrm{min}} G_{\mathrm{max}}$ (see Section 2.6.1). In **exciting** this quantity is called **rgkmax** and we keep this notation in the rest of this chapter. Furthermore, we need to set the $\boldsymbol{k}$-point mesh for the numerical integration in reciprocal space, which is done by specifying the parameter **ngridk**. For metallic systems the choice of the $\boldsymbol{k}$-point mesh is associated to the introduction of a smearing function. This function allows for a partial occupation of the states close to the Fermi energy. The width of the smearing function is given by the parameter **swidth**.

Some examples of these convergence tests can be found in Appendix B. As a result of the tests, we fix the parameter **rgkmax** = 8 for all calculations. The parameter **swidth** is set to 10^{-2} (10^{-4}) Ha for metallic (non-metallic) systems. Table 3.1 shows the chosen values for **ngridk**.

Table 3.1: Choosen $\boldsymbol{k}$-point mesh for the converged calculations.

ngridk	Elastic constants	Phonons
TiC	30×30×30	22×22×22
TiN	30×30×30	22×22×22
TiO - rutile	12×12×18	12×12×18
TiO - anatase	15×15×10	9×9×6

For self-consistent ground-state calculations, the default convergence criteria of **exciting** is used, which corresponds to total-energy variations of less than 10^{-6} Ha. When required, relaxation of the relative position of the atoms inside the unit cell is performed using the Broyden-Fletcher-Goldfarb-Shannon (**bfgs**) optimization method [20] with a threshold for the force of $2{\cdot}10^{-4}\,\mathrm{Ha}/a_{\mathrm{Bohr}}$.

3.2 Structural properties

To calculate elastic constants and phonon frequencies as described in the previous chapter, we first have to determine the equilibrium structure of the crystal. This requires both the search for the optimal shape and size of the unit cell and the relaxation of the relative positions of the atoms.

For systems which keep the cubic symmetry, only the volume has to be varied for finding the best unit cell. In this case, hydrostatic deformations are applied to the crystal to optimize the volume. The achieved energy-volume pairs are fitted using the Birch-Murnagham equation-of-state [21]:

$$E(\Omega) = E_0 + \frac{9\Omega_0 B_0}{16}\left\{\left[\left(\frac{\Omega_0}{\Omega}\right)^{\frac{2}{3}} - 1\right]^3 B_0' + \left[\left(\frac{\Omega_0}{\Omega}\right)^{\frac{2}{3}} - 1\right]^2 \left[6 - 4\left(\frac{\Omega_0}{\Omega}\right)^{\frac{2}{3}}\right]\right\}. \quad (3.2)$$

The search for the equilibrium structure of tetragonal systems needs more than a simple volume optimization. In this case, we alternately optimize the volume and the c/a-ratio. Tables 3.2 to 3.5 show our results for the equilibrium lattice parameters of the investigated systems. The obtained values agree well with theoretical and experimental results in the literature.

Table 3.2: Lattice constant a, bulk modulus B_0, and pressure derivative of the bulk modulus B_0' for TiC.

TiC		E_{xc}	a [Å]	B_0 [GPa]	B_0'
Present work		PBE	4.334	250.9	3.98
Theory	Ref. [22]	GGA	4.339	249.5	
	Ref. [23]	PBEsol	4.297	268	
	Ref. [24]	LDA	4.26	276.5	3.90
	Ref. [25]	PBE	4.331	249	
Experiment	Ref. [26]		4.328		
	Ref. [27]			242	
	Ref. [28]			233	

Table 3.3: Same as Table 3.2 for TiN.

TiN		E_{xc}	a [Å]	B_0 [GPa]	B_0'
Present work		`PBE`	4.248	276.0	4.24
Theory	Ref. [23]	`PBEsol`	4.210	300	
	Ref. [25]	`PBE`	4.246	279	
	Ref. [29]	`PBE`		294	
Experiment	Ref. [30]		4.247		
	Ref. [27]			277	

Table 3.4: Lattice constants a and c, bulk modulus B_0, and pressure derivative of the bulk modulus B_0' for TiO_2 in the rutile structure.

TiO_2 rutile		E_{xc}	a [Å]	c [Å]	B_0 [GPa]	B_0'
Present work		`PBE`	4.646	2.964	211.0	4.81
Theory	Ref. [31]	`GGA`	4.593	2.953	241	
	Ref. [32]	`LDA`	4.600	2.981	258	4.74
	Ref. [33]	`PBE`	4.705	2.966	235	4.64
Experiment	Ref. [34]		4.587	2.954		
	Ref. [35]		4.594	2.959	212	
	Ref. [36]				230	

Table 3.5: Same as Table 3.4 for the anatase structure.

TiO_2 anatase		E_{xc}	a [Å]	c [Å]	B_0 [GPa]	B_0'
Present work		`PBE`	3.799	9.710	186.5	4.50
Theory	Ref. [31]	`GGA`	3.759	9.585	175	
	Ref. [37]	`PBE`	3.797	9.789	177	4.13
Experiment	Ref. [34]		3.782	9.502		
	Ref. [38]		3.785	9.512	179	4.5

3.3 Elastic Constants

SOECs and TOECs are calculated using the **ElaStic** tool, which is introduced in Section 2.7. The required input for **ElaStic** is given by the optimized structures presented in the previous section. The initial $\eta_{\max}$ is set to 0.07 for every calculation and the number of strained structures is set to 57 for each deformation type. This leads to a distance of $\Delta\eta = 0.025$ between two consecutive deformation amplitudes. The values of the maximum strain and of the polynomial degree chosen for the fitting procedure used by **ElaStic** can be found in Appendix C.

3.3.1 Cubic systems

The studied crystals with cubic symmetry belong to the CI Laue group. The second-order stiffness tensor $\underline{\underline{\boldsymbol{c}}}^{(2)}_{\mathrm{CI}}$ in terms of Voigt indices has 3 independent elements: c_{11}, c_{12}, and c_{44} [2]. The full tensor can be represented as

$$\underline{\underline{\boldsymbol{c}}}^{(2)}_{\mathrm{CI}} = \begin{pmatrix} c_{11} & c_{12} & c_{12} & 0 & 0 & 0 \\ c_{12} & c_{11} & c_{12} & 0 & 0 & 0 \\ c_{12} & c_{12} & c_{11} & 0 & 0 & 0 \\ 0 & 0 & 0 & c_{44} & 0 & 0 \\ 0 & 0 & 0 & 0 & c_{44} & 0 \\ 0 & 0 & 0 & 0 & 0 & c_{44} \end{pmatrix} . \tag{3.3}$$

The third-order elastic tensor is a 6×6×6-matrix with 6 independent elastic constants for cubic systems. A representation of this tensor can be found in Appendix D. In order to calculate the matrix entries in Eq. (3.3), the deformations shown in Table 3.6 are used. Table 3.7 shows the deformations used to calculate the TOECs.

Table 3.6: Deformation types, expressed in the Voigt notation, that are used by **ElaStic** for cubic CI systems and SOECs. Here, the generic (i-th) strain tensor is represented as a vector $\boldsymbol{\eta}^{(i)} = (\eta_1, \eta_2, \eta_3, \eta_4, \eta_5, \eta_6)$.

$\boldsymbol{\eta}^{(i)}$	η_1	η_2	η_3	η_4	η_5	η_6
$\boldsymbol{\eta}^{(1)}$	η	η	η	0	0	0
$\boldsymbol{\eta}^{(2)}$	η	η	0	0	0	0
$\boldsymbol{\eta}^{(3)}$	0	0	0	2η	2η	2η

Table 3.7: Same as Table 3.6 for the calculation of the TOECs in cubic systems

$\boldsymbol{\eta}^{(i)}$	η_1	η_2	η_3	η_4	η_5	η_6
$\boldsymbol{\eta}^{(1)}$	η	η	η	0	0	0
$\boldsymbol{\eta}^{(2)}$	η	η	0	0	0	0
$\boldsymbol{\eta}^{(3)}$	0	0	0	2η	2η	2η
$\boldsymbol{\eta}^{(4)}$	η	η	$-\eta$	0	0	0
$\boldsymbol{\eta}^{(5)}$	η	0	0	2η	0	0
$\boldsymbol{\eta}^{(6)}$	η	0	0	0	2η	0

Table 3.8: Second-order elastic constants of TiC in units of [GPa].

TiC		E_{xc}	c_{11}	c_{12}	c_{44}
Present work		`PBE`	507.7	120.7	170.0
		`PBEsol`	483.1	119.4	161.6
Theory	Ref. [22]	`GGA`	509.3	119.2	169.5
	Ref. [24]	`LDA`	588	125	179
	Ref. [25]	`PBE`	519	115	183
	Ref. [39]	`PW91` [40]	470	97	167
Experiment	Ref. [41]		514.5	106.0	178.8
	Ref. [42]		500	113	175
	Ref. [43]		540	110	180
	Ref. [44]		510	100	180

Table 3.9: Same as Table 3.8 for TiN.

TiN		E_{xc}	c_{11}	c_{12}	c_{44}
Present work		`PBE`	578.0	124.8	165.2
		`PBEsol`	548.2	123.3	158.3
Theory	Ref. [45]	`PBE`	581	126	166
	Ref. [29]	`PBE`	590	145	169
	Ref. [25]	`PBE`	579	129	180
	Ref. [39]	`PW91`	610	100	168
Experiment	Ref. [39]		625	165	163
	Ref. [46]		507	96	163

Tables 3.8 and 3.9 show the SOECs of the cubic systems TiC and TiN and compare them with other calculations as well as experiments. As we can see, our values agree well with the literature. We also see that for c_{12} there are only minor differences between the different E_{xc} approximations, while for c_{11} and c_{44} the `PBEsol` calculations are around 5% lower than the results for `PBE`. Comparing the two materials, we see that TiN is the harder one. In particular, this is evident for the SOEC c_{11}, related to uniaxial and hydrostatic strain deformations.

Table 3.10: TOECs of the cubic systems TiC and TiN in units of [TPa].

		c_{111}	c_{112}	c_{123}	c_{144}	c_{155}	c_{456}
TiC	`PBE`	−7.38	−0.31	0.08	−0.05	−0.64	0.04
	`PBEsol`	−7.27	−0.30	0.08	−0.04	−0.62	0.04
TiN	`PBE`	−8.62	−0.45	0.36	0.07	−0.78	−0.04
	`PBEsol`	−8.48	−0.45	0.36	0.06	−0.76	−0.03

Table 3.10 shows the third-order elastic constants of cubic TiC and TiN. To the best of our knowledge, there are no further theoretical or experimental results available. The TOECs give a measure of how the SOECs change under the effects of strain. While the SOECs we calculate are obtained at equilibrium, they might change under certain deformations. As an example, we look at the strain deformation $\boldsymbol{\eta}^{(3)} = (0, 0, 0, 2\eta, 2\eta, 2\eta)^{\mathrm{T}}$. This deformation is directly related to the TOEC c_{456} and also to the SOEC c_{44} by

$$\frac{E_{(3)}(\eta)}{\Omega_0} = \frac{E_0}{\Omega_0} + 6\, c_{44}\, \eta^2 + 8\, c_{456}\, \eta^3 + \mathcal{O}(\eta^4). \tag{3.4}$$

Considering Eq. (3.4), an effective, strain-dependent $c_{44}^{(3)}(\eta)$ can be defined for the deformation $\boldsymbol{\eta}^{(3)}$ as:

$$c_{44}^{(3)}(\eta) = \frac{1}{12\,\Omega_0} \frac{\partial^2 E_{(3)}(\eta)}{\partial \eta^2} = c_{44} + 4\, c_{456}\, \eta + \mathcal{O}(\eta^2). \tag{3.5}$$

This means that for the strain deformation $\boldsymbol{\eta}^{(3)}$ the elastic constant c_{44} should increase for TiC and shrink for TiN by increasing the strain amplitude η.

3.3.2 Tetragonal structures

Both tetragonal TiO_2 structures, rutile and anatase, belong to the TI Laue group. The second-order stiffness tensor $\underline{\underline{\boldsymbol{c}}}^{(2)}_{\mathrm{TI}}$ has 6 independent elastic constants:

$$\underline{\underline{\boldsymbol{c}}}^{(2)}_{\mathrm{TI}} = \begin{pmatrix} c_{11} & c_{12} & c_{13} & 0 & 0 & 0 \\ c_{12} & c_{11} & c_{13} & 0 & 0 & 0 \\ c_{13} & c_{13} & c_{33} & 0 & 0 & 0 \\ 0 & 0 & 0 & c_{44} & 0 & 0 \\ 0 & 0 & 0 & 0 & c_{44} & 0 \\ 0 & 0 & 0 & 0 & 0 & c_{66} \end{pmatrix} . \tag{3.6}$$

In order to calculate these matrix entries, the strain deformations shown in Table 3.11 are used. Tables 3.12 and 3.13 shows the calculated SOECs for rutile and anatase, respectively.

Table 3.11: Deformation types, expressed in the Voigt notation, that are used by `ElaStic` for tetragonal TI systems and SOECs. Here, the generic (i-th) strain tensor is represented as a vector $\boldsymbol{\eta}^{(i)} = (\eta_1, \eta_2, \eta_3, \eta_4, \eta_5, \eta_6)$.

$\boldsymbol{\eta}^{(i)}$	η_1	η_2	η_3	η_4	η_5	η_6
$\boldsymbol{\eta}^{(1)}$	η	η	η	0	0	0
$\boldsymbol{\eta}^{(2)}$	$\frac{1}{2}\eta$	$\frac{1}{2}\eta$	$-\eta$	0	0	0
$\boldsymbol{\eta}^{(3)}$	η	$-\eta$	0	0	0	0
$\boldsymbol{\eta}^{(4)}$	0	0	η	0	0	0
$\boldsymbol{\eta}^{(5)}$	0	0	0	2η	0	0
$\boldsymbol{\eta}^{(6)}$	0	0	0	0	0	2η

Table 3.12: SOECs of TiO_2 in the rutile structure in units of [GPa].

TiO_2 rutile		E_{xc}	c_{11}	c_{12}	c_{13}	c_{33}	c_{44}	c_{66}
Present work		`PBE`	249.0	173.4	147.0	472.0	115.5	210.4
Theory	Ref. [33]	`PBE`	271	143	144	465	124	211
	Ref. [47]	`PBE`	278	153	149	479	115	214
	Ref. [32]	`LDA`	292	192	174	471	114	236
Experiment	Ref. [35]		267.3	174.1	146.4	483.9	123.9	190.4

Table 3.13: Same as Table 3.12 for the anatase structure.

TiO_2 anatase		E_{xc}	c_{11}	c_{12}	c_{13}	c_{33}	c_{44}	c_{66}
Present work		PBE	312.6	148.6	142.1	190.7	48.2	58.9
Theory	Ref. [37]	PBE	309.4	131	134	195	75	55
	Ref. [47]	PBE	320	151	143	190	54	60

Results of calculations for rutile and anatase show good agreement with the values in the literature. For most of the deformations the rutile phase seems to be harder than the anatase one. Compared to the cubic systems, we can see that they are harder than the tetragonal systems, as expected. However, the elastic constant c_{33} of rutile TiO_2 is nearly as high as c_{11} for the cubic systems.

The calculation of TOECs for tetragonal systems is not implemented in the published version of **ElaStic**. However, using the available total-energy calculations performed for the SOECs, we can calculate selected combinations of the TOECs. Table 3.14 shows the non-zero polynomial coefficients $A_3^{(i)}$ we obtain in this case.

Table 3.14: Non-zero coefficients $A_3^{(i)}$ used for second-order calculations (corresponding to the $\boldsymbol{\eta}^{(i)}$ in Table 3.11). The results are given in units of [TPa].

	rutile	anatase	expression in terms of TOECs
$A_3^{(1)}$	−4.47	−3.22	$\frac{1}{3}c_{111} + c_{112} + c_{113} + c_{123} + \frac{1}{6}c_{333}$
$A_3^{(2)}$	0.62	0.15	$\frac{1}{24}c_{111} + \frac{1}{8}c_{112} - \frac{1}{4}c_{113} - \frac{1}{4}c_{123} + \frac{1}{2}c_{133} - \frac{1}{6}c_{333}$
$A_3^{(4)}$	−0.74	−0.18	$\frac{1}{6}c_{333}$

We see, that the only TOEC which can be obtained directly from these deformations is c_{333}. For rutile (anatase) we get for c_{333} a value of −4.43 (−1.10) TPa.

3.3.3 New implementation in ElaStic

In order to calculate the full third-order tensor for tetragonal systems, we have extended the implementation of the calculation of the TOECs in **ElaStic** to the tetragonal TI symmetry. The third-order stiffness tensor for TI structures is taken from Table A.8 of Ref. [48]. The obtained elastic matrices are shown in Table 3.15.

Table 3.15: Two-dimensional matrix representation of TOECs for tetragonal TI structures.

$\underline{\underline{\boldsymbol{c}}}^{(3)}_{1jk}$

c_{111}	c_{112}	c_{113}	0	0	0
c_{112}	c_{112}	c_{123}	0	0	0
c_{113}	c_{123}	c_{133}	0	0	0
0	0	0	c_{144}	0	0
0	0	0	0	c_{155}	0
0	0	0	0	0	c_{166}

$\underline{\underline{\boldsymbol{c}}}^{(3)}_{2jk}$

c_{112}	c_{123}	c_{123}	0	0	0
c_{123}	c_{111}	c_{113}	0	0	0
c_{123}	c_{113}	c_{13}	0	0	0
0	0	0	c_{155}	0	0
0	0	0	0	c_{144}	0
0	0	0	0	0	c_{166}

$\underline{\underline{\boldsymbol{c}}}^{(3)}_{3jk}$

c_{113}	c_{123}	c_{133}	0	0	0
c_{123}	c_{113}	c_{133}	0	0	0
c_{133}	c_{133}	c_{333}	0	0	0
0	0	0	c_{344}	0	0
0	0	0	0	c_{344}	0
0	0	0	0	0	c_{366}

$\underline{\underline{\boldsymbol{c}}}^{(3)}_{4jk}$

0	0	0	c_{144}	0	0
0	0	0	c_{155}	0	0
0	0	0	c_{344}	0	0
c_{144}	c_{155}	c_{344}	0	0	0
0	0	0	0	0	c_{456}
0	0	0	0	c_{456}	0

$\underline{\underline{\boldsymbol{c}}}^{(3)}_{5jk}$

0	0	0	0	c_{155}	0
0	0	0	0	c_{144}	0
0	0	0	0	c_{344}	0
0	0	0	0	0	c_{456}
c_{155}	c_{144}	c_{344}	0	0	0
0	0	0	c_{456}	0	0

$\underline{\underline{\boldsymbol{c}}}^{(3)}_{6jk}$

0	0	0	0	0	c_{166}
0	0	0	0	0	c_{166}
0	0	0	0	0	c_{366}
0	0	0	0	c_{456}	0
0	0	0	c_{456}	0	0
c_{155}	c_{144}	c_{344}	0	0	0

Table 3.16: Deformation types, expressed in the Voigt notation, that are used by **ElaStic** for tetragonal TI systems and TOECs. Here, the generic (i-th) strain tensor is represented as a vector $\boldsymbol{\eta}^{(i)} = (\eta_1, \eta_2, \eta_3, \eta_4, \eta_5, \eta_6)$.

$\boldsymbol{\eta}^{(i)}$	η_1	η_2	η_3	η_4	η_5	η_6
$\boldsymbol{\eta}^{(1)}$	η	0	0	0	0	0
$\boldsymbol{\eta}^{(2)}$	η	η	0	0	0	0
$\boldsymbol{\eta}^{(3)}$	0	0	η	0	0	0
$\boldsymbol{\eta}^{(4)}$	0	0	η	2η	2η	0
$\boldsymbol{\eta}^{(5)}$	0	η	0	0	0	2η
$\boldsymbol{\eta}^{(6)}$	η	0	0	0	2η	0
$\boldsymbol{\eta}^{(7)}$	0	η	0	0	2η	0
$\boldsymbol{\eta}^{(8)}$	0	η	η	0	0	0
$\boldsymbol{\eta}^{(9)}$	0	0	η	0	0	2η
$\boldsymbol{\eta}^{(10)}$	η	η	η	0	0	0
$\boldsymbol{\eta}^{(11)}$	η	η	$-\eta$	0	0	0
$\boldsymbol{\eta}^{(12)}$	0	0	0	2η	2η	2η

For the selection of deformation types, we use a variation of Table 2 from Ref. [49], shown in Table 3.16. Employing these deformations, the TOECs shown in Table 3.15 can be expressed as a function of the third-order fitting coefficients as displayed in Table 3.17. The TOECs of the rutile phase of TiO_2 obtained with this new implementation of **ElaStic** are given in Table 3.18.

Table 3.17: TOECs and their expression integers in terms of the fitting coefficients $A_3^{(i)}$, for tetragonal TI systems.

c_{111}	$6A_3^{(1)}$	c_{155}	$\frac{1}{2}\left(A_3^{(6)} - A_3^{(1)}\right)$
c_{112}	$A_3^{(2)} - 2A_3^{(1)}$	c_{166}	$\frac{1}{2}\left(A_3^{(5)} - A_3^{(1)}\right)$
c_{113}	$A_3^{(2)} - 2\left(A_3^{(1)} + A_3^{(3)} - A_3^{(8)}\right) - \frac{1}{2}\left(A_3^{(10)} - A_3^{(11)}\right)$	c_{333}	$6A_3^{(3)}$
c_{123}	$2\left(A_3^{(1)} - A_3^{(8)}\right) - A_3^{(2)} + A_3^{(3)} + A_3^{(10)}$	c_{344}	$\frac{1}{4}\left(A_3^{(4)} - A_3^{(3)}\right)$
c_{133}	$\frac{1}{2}\left(A_3^{(10)} + A_3^{(11)}\right) - A_3^{(2)}$	c_{366}	$\frac{1}{2}\left(A_3^{(9)} - A_3^{(3)}\right)$
c_{144}	$\frac{1}{2}\left(A_3^{(7)} - A_3^{(1)}\right)$	c_{456}	$\frac{1}{8}A_3^{(12)}$

Table 3.18: TOECs for the rutile structure of TiO_2 in units of [TPa], as obtained from the new implementation of **ElaStic**. Calculations are performed using a maximum strain value of 0.15 and 61 strain points.

c_{111}	c_{112}	c_{113}	c_{123}	c_{133}	c_{144}
−1.33	−1.58	0.38	−1.69	−0.41	−0.28
c_{155}	c_{166}	c_{333}	c_{344}	c_{366}	c_{456}
−0.44	−1.25	−4.38	−0.40	−0.58	−0.26

As a cross check, in Table 3.19, we compare the fitting coefficients of Table 3.14 and the ones obtained by using the TOECs from Table 3.18. The minor differences that we see in Table 3.19 can be ascribed to the choice of slightly different values of the maximum strain.

Table 3.19: Comparison of the third-order fitting coefficients $A_3^{(i)}$ calculated using the new implementation of **ElaStic** and the data extracted from the second-order calculations. Units are [TPa].

	new implementation	from Table 3.14
$A_3^{(1)}$	−4.06	−4.47
$A_3^{(2)}$	0.60	0.62
$A_3^{(4)}$	−0.73	−0.74

3.4 Lattice-dynamical properties

To calculate the phonon frequencies, **exciting** uses the frozen-phonon approach. To this purpose, atomic positions are shifted according to collective displacements with a given periodicity, determined by the phonon wavevector $\boldsymbol{q}$. Then, the total energy and forces are calculated by **exciting** for the displaced structure. From the knowledge of the forces of several displacement patterns, the interatomic force constants and, in turn, the dynamical matrix for the given value of $\boldsymbol{q}$ are obtained. This matrix is then symmetrized and diagonalized. This yields the eigenvalues and eigenvectors. The square root of the eigenvalues, then, gives the phonon frequencies.

In this thesis, we focus our interest on the phonon frequencies at the center of the Brillouin zone ($\boldsymbol{q}$=0). In this case, no "expensive" supercell calculation is needed. However, due to the periodic boundary conditions used in **exciting**, only frequencies corresponding to transverse-optical (TO) modes can be obtained. For

polar materials, then, we have the drawback that longitudinal-optical (LO) and TO modes become degenerate and no LO-TO splitting can be obtained. Therefore, we focus our investigation only to TO frequencies. For metallic systems, nevertheless, there is no LO-TO splitting.

For the cubic systems there are 6 independent modes at each value of $\boldsymbol{q}$. At the Γ point ($\boldsymbol{q}$=0), the frequencies of the three acoustic modes vanish. Therefore, only the three optical mode are considered for TiC and TiN. These cubic systems are metallic, therefore, all optical frequencies are degenerate at Γ, with a value denoted $\omega_{\text{opt}}(\Gamma)$. To calculate the mode Grüneisen parameter for the cubic systems, the volume of the crystal is changed. Then, phonon calculations are performed for slightly different ($\pm 0.5\%$) values of the lattice constant a. Numerical derivation of the obtained phonon frequencies leads to the mode Grüneisen parameters as introduced in Section 2.2.2. Table 3.20 shows our results for TiN and TiC.

Table 3.20: Optical phonon frequency $\omega_{\text{opt}}(\Gamma)$ in units of [cm^{-1}] and mode Grüneisen parameters $\gamma_{\text{opt}}(\Gamma)$ for TiC and TiN at the Γ point.

		E_{xc}	TiC		TiN	
			$\omega_{\text{opt}}(\Gamma)$	$\gamma_{\text{opt}}(\Gamma)$	$\omega_{\text{opt}}(\Gamma)$	$\gamma_{\text{opt}}(\Gamma)$
Present work		`PBE`	513	1.9	505	2.2
		`PBEsol`	511		502	
Theory	Ref. [24]	`LDA`	507			
	Ref. [50]	`PBE`			545	
Experiment	Ref. [43]		537			
	Ref. [28]			1.9		
	Ref. [51]				484	

As we can see from Table 3.20, the optical modes of TiC and TiN are quite similar. The value of the mode Grüneisen parameter $\gamma_{\text{opt}}(\Gamma)$ of TiN is higher than for TiC. This indicates a stronger change of the phonon frequency $\omega_{\text{opt}}(\Gamma)$ in terms of changes in the volume.

The anatase phase of TiO_2 has a primitive unit cell which contains 6 atoms. Therefore, there are 18 independent modes at each $\boldsymbol{q}$ point. Again, the three acoustic modes at Γ have vanishing frequency. Taken into account degenerate modes, the number of resulting pure TO frequencies at Γ is 10. Table 3.21 shows the frequencies of the pure TO modes for the anatase phase of TiO_2.

Table 3.21: TO phonon frequencies at Γ for TiO_2 in the anatase structure. All frequencies are in units of [cm^{-1}].

Mulliken notation	Present work	Ref. [31]	Ref. [52]	
	PBE	GGA	GGA	Expt.
E_g	128	105	157	143
E_g	166	165	191	198
E_u	219	240	263	262
A_{2u}	337	402	334	367
B_{1g}	380	465	381	395
E_u	420	465	432	435
B_{1g}	497	518	520	512
A_{1g}	516	535	518	518
B_{2u}	543	574	542	
E_g	620	655	641	639

3.5 Comparison of the studied Ti compounds

In order to compare the elastic properties of the materials which we investigated, we look at the elastic moduli, which can be expressed by linear combinations of SOECs in the Voigt approach [53]. These moduli are the bulk modulus B introduced in Section 3.1, the shear modulus G, the Young modulus E connected to changes in length along a direction, and the Poisson ratio ν_p representing the transversal expansion due to an axial compression. Table 3.22 shows the value of these moduli, calculated with the obtained SOECs.

Table 3.22: Bulk modulus B, shear modulus G, Young modulus E, and Poisson ratio ν_p for all investigated materials. Only PBE results are included.

	B [GPa]	G [GPa]	E [GPa]	ν_p
TiC	249.7	179.4	434.3	0.21
TiN	275.8	189.8	463.1	0.22
TiO_2 rutile	211.6	121.8	306.6	0.26
TiO_2 anatase	186.9	56.6	154.3	0.36

As expected, the values of the bulk modulus are consistent with the ones calculated using Eq. (3.2) in Section 3.2. Comparing the values for each material, we see that the cubic crystals are harder than the TiO_2 structures, with TiN being the hardest

and the anatase structure of TiO_2 the softest one. According to the Pugh's rule [54], the value of G/B is related to ductility and brittleness. Materials with $G/B > 0.5$ have brittle behavior. This is the case for TiN, TiC, and rutile TiO_2. TiO_2 in the anatase phase, however, should behave ductile. The rule proposed by Frantsevich and coworkers [55], which claims that materials with a Poisson ratio $\nu > 0.33$ should be ductile, reaches the same conclusion.

Comparing the phonon frequencies of the cubic systems TiC and TiN, we see that they have nearly the same frequency. Because they have the same structure and carbon and nitrogen nearly the same physical properties (mass, charge) this is reasonable. Comparing the cubic system with anatase is not that easy, due to the fact that it is a completely different structure. The primitive unit cell of anatase has a volume which is about 3.4 times larger than the ones for TiC and TiN. Even having 6 atoms per primitive unit cell, the particle density of anatas is lower than for the cubic systems, which leads to a less compact structure. Furthermore, the oxygen atom has a mass which is about 33% larger than the carbon one. These two facts can lead to smaller frequencies for the anatase TiO_2 phase. We can see this result in the low-frequency modes, where mostly both Ti and O atoms are oscillating. The high-frequency modes in anatase TiO_2 have frequencies comparable to the cubic systems and are characterized by vibrations of only the oxygen atoms.

4. Conclusions and outlook

In this work, the elastic and lattice dynamical properties of a set of four titanium compounds have been investigated from first principles using the program **exciting** and the **ElaStic** toolkit.

For TiC, TiN, and TiO_2 in the rutile and anatase phase, the full tensor of the second-order elastic constants (SOECs) has been obtained, with a good agreement with the existing literature. In addition to this, the third-order elastic constants (TOECs) of cubic TiC and TiN as well as TiO_2 in the rutile phase have been calculated for the first time, to the best of our knowledge. In order to perform the calculation of TOECs for the tetragonal phases, we have extended the **ElaStic** toolkit with our implementation for the TI Laue group. The calculated SOECs and TOECs can be used for predicting the behaviour of the selected materials under any applied strain to a large extent of the elastic-regime region.

At the Γ point, optical phonon frequencies and mode Grüneisen parameters of the cubic TiC and TiN have been calculated. The full set of pure transverse-optical phonon frequencies at the zone centre for TiO_2 in the anatase phase has been obtained and compared with data from the literature.

In the further extension of this work, phonon frequencies and mode Grüneisen parameters should be obtained in the full Brillouin zone, at least for cubic structures. This extension would allow for the calculation of the linear expansion coefficient of these systems as a function of the temperature. The knowledge of the expansion coefficient is a crucial step for the prediction of the behaviour of materials at high temperature.

Finally, from the point of view of the elastic properties, the new implementation in **ElaStic** will allow for the calculation of non-linear elastic constants not only for the anatase phase of TiO_2, but also for other tetragonal structures.

Bibliography

[1] Gulans, A. ; Kontur, S. ; Meisenbichler, C. ; Nabok, D. ; Pavone, P. ; Rigamonti, S. ; Sagmeister, S. ; Werner, U. ; Draxl, C.: *exciting: a full-potential all-electron package implementing density-functional theory and many-body perturbation theory*. Journal of Physics: Condensed Matter 26 (2014), Nr. 36, 363202. http://stacks.iop.org/0953-8984/26/i=36/a=363202

[2] Golesorkhtabar, R. ; Pavone, P. ; Spitaler, J. ; Puschnig, P. ; Draxl, C.: *ElaStic: A tool for calculating second-order elastic constants from first principles*. Computer Physics Communications 184 (2013), Nr. 8, 1861 - 1873. http://dx.doi.org/https://doi.org/10.1016/j.cpc.2013.03.010

[3] Toth, L.: *Transition Metal Carbides and Nitrides*. Academic Press, 1971

[4] https://www.britannica.com/technology/titanium-processing

[5] http://www.rsc.org/learn-chemistry/resource/download/res00001268/cmp00002618/pdf

[6] Giustino, F.: *Materials Modelling using Density Functional Theory*. Oxford University Press, 2014

[7] Wahab, D. M. A.: *Solid state physics*. Narosa Publishing House, 1999

[8] Timoshenko, S. ; Goodier, J. N.: *Theory of Elasticity*. McGRAW-HILL BOOK COMPANY, 1951

[9] Grimvall, G. ; Wohlfarth, E. (Hrsg.): *Thermophysical properties of materials*. Elsevier Science Publischer, 1986

[10] Brugger, K.: *Thermodynamic Definition of Higher Order Elastic Coefficients*. Phys. Rev. 133 (1964), Mar, A1611–A1612. http://dx.doi.org/10.1103/PhysRev.133.A1611

[11] Born, M. ; Oppenheimer, R.: *Zur Quantentheorie der Molekeln.* Annalen der Physik 389 (1927), Nr. 20, 457-484. http://dx.doi.org/10.1002/andp.19273892002

[12] Hohenberg, P. ; Kohn, W.: *Inhomogeneous Electron Gas.* Phys. Rev. 136 (1964), Nov, B864–B871. http://dx.doi.org/10.1103/PhysRev.136.B864

[13] Kohn, W. ; Sham, L. J.: *Self-Consistent Equations Including Exchange and Correlation Effects.* Phys. Rev. 140 (1965), Nov, A1133–A1138. http://dx.doi.org/10.1103/PhysRev.140.A1133

[14] Nguyen-Dang, T. T. ; Bader, R. F. W. ; Essén, H.: *Some properties of the Lagrange multiplier μ in density functional theory.* International Journal of Quantum Chemistry 22 (1982), Nr. 5, 1049-1058. http://dx.doi.org/doi:10.1002/qua.560220517

[15] Perdew, J. P. ; Schmidt, K.: *Jacob's ladder of density functional approximations for the exchange-correlation energy.* AIP Conference Proceedings 577 (2001), Nr. 1, 1-20. http://dx.doi.org/10.1063/1.1390175

[16] Yanchitsky, B. ; Timoshevskii, A.: *Determination of the space group and unit cell for a periodic solid This program can be downloaded from the CPC Program Library under catalogue identifier: http://cpc.cs.qub.ac.uk/summaries/ADON.* Computer Physics Communications 139 (2001), Nr. 2, 235 - 242. http://dx.doi.org/https://doi.org/10.1016/S0010-4655(01)00212-0

[17] Perdew, J. P. ; Burke, K. ; Ernzerhof, M.: *Generalized Gradient Approximation Made Simple.* Phys. Rev. Lett. 77 (1996), Oct, 3865–3868. http://dx.doi.org/10.1103/PhysRevLett.77.3865

[18] Perdew, J. P. ; Ruzsinszky, A. ; Csonka, G. I. ; Vydrov, O. A. ; Scuseria, G. E. ; Constantin, L. A. ; Zhou, X. ; Burke, K.: *Restoring the Density-Gradient Expansion for Exchange in Solids and Surfaces.* Phys. Rev. Lett. 100 (2008), April, S. 136406. http://dx.doi.org/10.1103/PhysRevLett.100.136406

[19] Råsander, M. ; Moram, M. A.: *On the accuracy of commonly used density functional approximations in determining the elastic constants of insulators and semiconductors.* The Journal of Chemical Physics 143 (2015), Nr. 14, 144104. http://dx.doi.org/10.1063/1.4932334

[20] Byrd, R. ; Lu, P. ; Nocedal, J. ; Zhu, C.: *A Limited Memory Algorithm for Bound Constrained Optimization.* SIAM Journal on Scientific Computing 16 (1995), Nr. 5, 1190-1208. http://dx.doi.org/10.1137/0916069

[21] Birch, F.: *Finite Elastic Strain of Cubic Crystals.* Phys. Rev. 71 (1947), Jun, 809–824. http://dx.doi.org/10.1103/PhysRev.71.809

[22] Chen, L. ; Wang, Q. ; Xiong, L. ; Gong, H.: *Mechanical properties and point defects of MC (M=Ti, Zr) from first-principles calculation.* Journal of Alloys and Compounds 747 (2018), 972 - 977. http://dx.doi.org/https://doi.org/10.1016/j.jallcom.2018.03.047

[23] Gautam, G. S. ; Kumar, K. H.: *Elastic, thermochemical and thermophysical properties of rock salt-type transition metal carbides and nitrides: A first principles study.* Journal of Alloys and Compounds 587 (2014), 380 - 386. http://dx.doi.org/https://doi.org/10.1016/j.jallcom.2013.10.156

[24] Bağci, S. ; Kamiş, T. ; Tütüncü, H. ; P. Srivastava, G.: *Ab initio calculation of phonons for bulk TiC and TiC(001)(1X1).* Phys. Rev. B 80 (2009), 07. http://dx.doi.org/10.1103/PhysRevB.80.035405

[25] Yang, Y. ; Lu, H. ; Yu, C. ; Chen, J.: *First-principles calculations of mechanical properties of TiC and TiN.* Journal of Alloys and Compounds 485 (2009), Nr. 1, 542 - 547. http://dx.doi.org/https://doi.org/10.1016/j.jallcom.2009.06.023

[26] Strzęciwilk, D. ; Wokulski, Z. ; Tkacz, P.: *Microstructure of TiC crystals obtained from high temperature nickel solution.* Journal of Alloys and Compounds 350 (2003), Nr. 1, 256 - 263. http://dx.doi.org/https://doi.org/10.1016/S0925-8388(02)00955-6

[27] Yang, Q. ; Lengauer, W. ; Koch, T. ; Scheerer, M. ; Smid, I.: *Hardness and elastic properties of Ti(CxN1-x), Zr(CxN1-x) and Hf(CxN1-x).* Journal of Alloys and Compounds 309 (2000), Nr. 1, L5 - L9. http://dx.doi.org/https://doi.org/10.1016/S0925-8388(00)01057-4

[28] Dodd, S. P. ; Cankurtaran, M. ; James, B.: *Ultrasonic determination of the elastic and nonlinear acoustic properties of transition-metal carbide ceramics: TiC and TaC.* Journal of Materials Science 38 (2003), Mar, Nr. 6, 1107–1115. http://dx.doi.org/10.1023/A:1022845109930

[29] Yu, S. ; Zeng, Q. ; Oganov, A. R. ; Frapper, G. ; Zhang, L.: *Phase stability, chemical bonding and mechanical properties of titanium nitrides: a first-principles study.* Phys. Chem. Chem. Phys. 17 (2015), 11763-11769. http://dx.doi.org/10.1039/C5CP00156K

[30] Schoenberg, N.: *An X-ray investigation on ternary phases in the Ta-Me-N systems (Me = Ti, Cr, Mn, Fe, Co, Ni).* Acta Chemica Scandinavica (1-27,1973-42,1988) 8 (1954), 213-220. http://actachemscand.org/pdf/acta_vol_08_p0213-0220.pdf?fbclid=IwAR2zk5dwaMG9pBlcXtWNdVkShUk5vPg40GJb7L6XF3G4Y_g-HXBZ2MdqjOY

[31] Mei, Z.-G. ; Wang, Y. ; Shang, S.-L. ; Liu, Z.-K.: *First-Principles Study of Lattice Dynamics and Thermodynamics of TiO2 Polymorphs.* Inorganic Chemistry 50 (2011), Nr. 15, 6996-7003. http://dx.doi.org/10.1021/ic200349p

[32] Jun, Z. ; Jing-Xin, Y. ; Yan-Ju, W. ; Xiang-Rong, C. ; Fu-Qian, J.: *First-principles calculations for elastic properties of rutile TiO 2 under pressure.* Chinese Physics B 17 (2008), Nr. 6, 2216. http://stacks.iop.org/1674-1056/17/i=6/a=046

[33] Mahmood, T. ; Cao, C. ; Khan, W. S. ; Usman, Z. ; Butt, F. K. ; Hussain, S.: *Electronic, elastic, optical properties of rutile TiO2 under pressure: A DFT study.* Physica B: Condensed Matter 407 (2012), Nr. 6, 958 - 965. http://dx.doi.org/https://doi.org/10.1016/j.physb.2011.12.114

[34] Burdett, J. K. ; Hughbanks, T. ; Miller, G. J. ; Richardson, J. W. ; Smith, J. V.: *Structural-electronic relationships in inorganic solids: powder neutron diffraction studies of the rutile and anatase polymorphs of titanium dioxide at 15 and 295 K.* Journal of the American Chemical Society 109 (1987), Nr. 12, 3639-3646. http://dx.doi.org/10.1021/ja00246a021

[35] Isaak, D. G. ; Carnes, J. D. ; Anderson, O. L. ; Cynn, H. ; Hake, E.: *Elasticity of TiO2 rutile to 1800 K.* Physics and Chemistry of Minerals 26 (1998), Nov, Nr. 1, 31–43. http://dx.doi.org/10.1007/s002690050158

[36] Gerward, L. ; Staun Olsen, J.: *Post-Rutile High-Pressure Phases in TiO_2.* Journal of Applied Crystallography 30 (1997), Jun, Nr. 3, 259–264. http://dx.doi.org/10.1107/S0021889896011454

[37] Mahmood, T. ; Malik, H. ; Batool, R. ; Perveen, Z. ; Saleemi, F. ; Rasheed, H. ; Saeed, M. ; Cao, C. ; Rizwan, M.: *Elastic, electronic and optical properties of anatase TiO2 under pressure: A*

DFT approach. Chinese Journal of Physics 55 (2017), Nr. 4, 1252 - 1263. http://dx.doi.org/https://doi.org/10.1016/j.cjph.2017.05.029

[38] Arlt, T. ; Bermejo, M. ; Blanco, M. A. ; Gerward, L. ; Jiang, J. Z. ; Staun Olsen, J. ; Recio, J. M.: *High-pressure polymorphs of anatase* TiO_2. Phys. Rev. B 61 (2000), Jun, 14414–14419. http://dx.doi.org/10.1103/PhysRevB.61.14414

[39] Ahuja, R. ; Eriksson, O. ; Wills, J. M. ; Johansson, B.: *Structural, elastic, and high-pressure properties of cubic TiC, TiN, and TiO*. Phys. Rev. B 53 (1996), Feb, 3072–3079. http://dx.doi.org/10.1103/PhysRevB.53.3072

[40] Perdew, J. P. ; Chevary, J. A. ; Vosko, S. H. ; Jackson, K. A. ; Pederson, M. R. ; Singh, D. J. ; Fiolhais, C.: *Atoms, molecules, solids, and surfaces: Applications of the generalized gradient approximation for exchange and correlation*. Phys. Rev. B 46 (1992), Sep, 6671–6687. http://dx.doi.org/10.1103/PhysRevB.46.6671

[41] Chang, R. ; Graham, L. J.: *Low-Temperature Elastic Properties of ZrC and TiC*. Journal of Applied Physics 37 (1966), Nr. 10, 3778-3783. http://dx.doi.org/10.1063/1.1707923

[42] Gilman, J. J. ; Roberts, B. W.: *Elastic Constants of TiC and TiB2*. Journal of Applied Physics 32 (1961), Nr. 7, 1405-1405. http://dx.doi.org/10.1063/1.1736249

[43] Pintschovius, L. ; Reichardt, W. ; Scheerer, B.: *Lattice dynamics of TiC*. Journal of Physics C: Solid State Physics 11 (1978), Nr. 8, 1557. http://stacks.iop.org/0022-3719/11/i=8/a=016

[44] Weber, W.: *Lattice Dynamics of Transition-Metal Carbides*. Phys. Rev. B 8 (1973), Dec, 5082–5092. http://dx.doi.org/10.1103/PhysRevB.8.5082

[45] Yang, R. ; Zhu, C. ; Wei, Q. ; Xiao, K. ; Du, Z.: *First-principles study of optical, elastic anisotropic and thermodynamic properties of TiN under high temperature and high pressure*. Condensed Matter Physics 20 (2017), 06, S. 23601. http://dx.doi.org/10.5488/CMP.20.23601

[46] Meng, W. ; Eesley, G.: *Growth and mechanical anisotropy of TiN thin films*. Thin Solid Films 271 (1995), Nr. 1, 108 - 116. http://dx.doi.org/https://doi.org/10.1016/0040-6090(95)06875-9

[47] Iuga, M. ; Steinle-Neumann, G. ; Meinhardt, J.: *Ab-initio simulation of elastic constants for some ceramic materials.* Eur. Phys. J. B 58 (2007), Nr. 2, 127-133. http://dx.doi.org/10.1140/epjb/e2007-00209-1

[48] Clayton, J. D.: *Nonlinear Mechanics of Crystals.* Springer Netherlands, 2011

[49] Yang, H. ; Huang, W. Q.: *Theoretical Predication Method of High Order Elastic Constants of Cubic and Tetragonal Crystal Material.* In: *Research in Materials and Manufacturing Technologies* Bd. 834, Trans Tech Publications, 1 2014 (Advanced Materials Research), S. 263–267

[50] Isaev, E. I. ; Simak, S. I. ; Abrikosov, I. A. ; Ahuja, R. ; Vekilov, Y. K. ; Katsnelson, M. I. ; Lichtenstein, A. I. ; Johansson, B.: *Phonon related properties of transition metals, their carbides, and nitrides: A first-principles study.* Journal of Applied Physics 101 (2007), Nr. 12, 123519. http://dx.doi.org/10.1063/1.2747230

[51] Kress, W. ; Roedhammer, P. ; Bilz, H. ; Teuchert, W. D. ; Christensen, A. N.: *Phonon anomalies in transition-metal nitrides: TiN.* Phys. Rev. B 17 (1978), Jan, 111–113. http://dx.doi.org/10.1103/PhysRevB.17.111

[52] Giarola, M. ; Sanson, A. ; Monti, F. ; Mariotto, G. ; Bettinelli, M. ; Speghini, A. ; Salviulo, G.: *Vibrational dynamics of anatase TiO_2: Polarized Raman spectroscopy and ab initio calculations.* Phys. Rev. B 81 (2010), May, 174305. http://dx.doi.org/10.1103/PhysRevB.81.174305

[53] Voigt, W.: *Lehrbuch der Kristallphysik (mit Ausschluss der Kristalloptik).* Teubner Verlag, 1928

[54] Pugh, S.: *XCII. Relations between the elastic moduli and the plastic properties of polycrystalline pure metals.* The London, Edinburgh, and Dublin Philosophical Magazine and Journal of Science 45 (1954), Nr. 367, 823-843. http://dx.doi.org/10.1080/14786440808520496

[55] I. N. Frantsevich, F. F. V. ; Bokuta, S. A. ; Frantsevich, I. N. (Hrsg.): *Elastic Constants and Elastic Moduli of Metals and Insulators Handbook.* Naukova Dumka, Kiev, 1983

A. Species files

- **Species file for the element Carbon**

```
<?xml version="1.0" encoding="UTF-8"?>
<spdb xsi:noNamespaceSchemaLocation="../../xml/species.xsd" xmlns:xsi="
   http://www.w3.org/2001/XMLSchema-instance">
  <sp chemicalSymbol="C" name="carbon" z="-6.00000" mass="21894.16673">
    <muffinTin rmin="0.100000E-04" radius="1.4500" rinf="21.0932"
       radialmeshPoints="250"/>
    <atomicState n="1" l="0" kappa="1" occ="2.00000" core="true"/>
    <atomicState n="2" l="0" kappa="1" occ="2.00000" core="false"/>
    <atomicState n="2" l="1" kappa="1" occ="1.00000" core="false"/>
    <atomicState n="2" l="1" kappa="2" occ="1.00000" core="false"/>
    <basis>
      <default type="lapw" trialEnergy="0.1500" searchE="false"/>
      <custom l="0" type="lapw" trialEnergy="0.1500" searchE="true"/>
      <lo l="0">
        <wf matchingOrder="0" trialEnergy="0.15" searchE="true"/>
        <wf matchingOrder="1" trialEnergy="0.15" searchE="true"/>
      </lo>
      <lo l="0">
        <wf matchingOrder="0" trialEnergy="0.15" searchE="true"/>
        <wf matchingOrder="2" trialEnergy="0.15" searchE="true"/>
      </lo>
      <custom l="1" type="lapw" trialEnergy="0.3800" searchE="true"/>
      <lo l="1">
        <wf matchingOrder="0" trialEnergy="0.38" searchE="true"/>
        <wf matchingOrder="1" trialEnergy="0.38" searchE="true"/>
      </lo>
      <lo l="1">
        <wf matchingOrder="0" trialEnergy="0.38" searchE="true"/>
        <wf matchingOrder="2" trialEnergy="0.38" searchE="true"/>
      </lo>
    </basis>
  </sp>
</spdb>
```

- **Species file for the element Nitrogen**

```
<?xml version="1.0" encoding="UTF-8"?>
<spdb xsi:noNamespaceSchemaLocation="../../xml/species.xsd" xmlns:xsi="
    http://www.w3.org/2001/XMLSchema-instance">
  <sp chemicalSymbol="N" name="nitrogen" z="-7.00000" mass="25532.72506
      ">
    <muffinTin rmin="0.100000E-04" radius="1.4500" rinf="18.9090"
       radialmeshPoints="250"/>
    <atomicState n="1" l="0" kappa="1" occ="2.00000" core="true"/>
    <atomicState n="2" l="0" kappa="1" occ="2.00000" core="false"/>
    <atomicState n="2" l="1" kappa="1" occ="1.00000" core="false"/>
    <atomicState n="2" l="1" kappa="2" occ="2.00000" core="false"/>
    <basis>
      <default type="lapw" trialEnergy="0.1500" searchE="false"/>
      <custom l="0" type="lapw" trialEnergy="0.1500" searchE="true"/>
      <lo l="0">
        <wf matchingOrder="0" trialEnergy="0.15" searchE="true"/>
        <wf matchingOrder="1" trialEnergy="0.15" searchE="true"/>
      </lo>
      <lo l="0">
        <wf matchingOrder="0" trialEnergy="0.15" searchE="true"/>
        <wf matchingOrder="2" trialEnergy="0.15" searchE="true"/>
      </lo>
      <custom l="1" type="lapw" trialEnergy="0.1500" searchE="true"/>
      <lo l="1">
        <wf matchingOrder="0" trialEnergy="0.15" searchE="true"/>
        <wf matchingOrder="1" trialEnergy="0.15" searchE="true"/>
      </lo>
      <lo l="1">
        <wf matchingOrder="0" trialEnergy="0.15" searchE="true"/>
        <wf matchingOrder="2" trialEnergy="0.15" searchE="true"/>
      </lo>
    </basis>
  </sp>
</spdb>
```

- **Species file for the element Oxygen**

```
<?xml version="1.0" encoding="UTF-8"?>
<spdb xsi:noNamespaceSchemaLocation="../../xml/species.xsd" xmlns:xsi="
    http://www.w3.org/2001/XMLSchema-instance">
  <sp chemicalSymbol="O" name="oxygen" z="-8.00000" mass="29165.12203">
    <muffinTin rmin="0.100000E-04" radius="1.4500" rinf="17.0873"
       radialmeshPoints="250"/>
    <atomicState n="1" l="0" kappa="1" occ="2.00000" core="true"/>
    <atomicState n="2" l="0" kappa="1" occ="2.00000" core="false"/>
    <atomicState n="2" l="1" kappa="1" occ="2.00000" core="false"/>
    <atomicState n="2" l="1" kappa="2" occ="2.00000" core="false"/>
    <basis>
      <default type="lapw" trialEnergy="0.1500" searchE="false"/>
      <custom l="0" type="lapw" trialEnergy="0.1500" searchE="true"/>
      <lo l="0">
        <wf matchingOrder="0" trialEnergy="0.15" searchE="true"/>
        <wf matchingOrder="1" trialEnergy="0.15" searchE="true"/>
      </lo>
      <lo l="0">
        <wf matchingOrder="0" trialEnergy="0.15" searchE="true"/>
        <wf matchingOrder="2" trialEnergy="0.15" searchE="true"/>
      </lo>
      <custom l="1" type="lapw" trialEnergy="0.1500" searchE="true"/>
      <lo l="1">
        <wf matchingOrder="0" trialEnergy="0.15" searchE="true"/>
        <wf matchingOrder="1" trialEnergy="0.15" searchE="true"/>
      </lo>
      <lo l="1">
        <wf matchingOrder="0" trialEnergy="0.15" searchE="true"/>
        <wf matchingOrder="2" trialEnergy="0.15" searchE="true"/>
      </lo>
    </basis>
  </sp>
</spdb>
```

- **Species file for the element Titanium**

```
<?xml version="1.0" encoding="UTF-8"?>
<spdb xsi:noNamespaceSchemaLocation="../../xml/species.xsd" xmlns:xsi="
    http://www.w3.org/2001/XMLSchema-instance">
  <sp chemicalSymbol="Ti" name="titanium" z="-22.0000" mass="
      87256.20311">
    <muffinTin rmin="0.100000E-04" radius="2.0000" rinf="25.7965"
       radialmeshPoints="350"/>
    <atomicState n="1" l="0" kappa="1" occ="2.00000" core="true"/>
    <atomicState n="2" l="0" kappa="1" occ="2.00000" core="true"/>
    <atomicState n="2" l="1" kappa="1" occ="2.00000" core="true"/>
    <atomicState n="2" l="1" kappa="2" occ="4.00000" core="true"/>
    <atomicState n="3" l="0" kappa="1" occ="2.00000" core="false"/>
    <atomicState n="3" l="1" kappa="1" occ="2.00000" core="false"/>
    <atomicState n="3" l="1" kappa="2" occ="4.00000" core="false"/>
    <atomicState n="3" l="2" kappa="2" occ="2.00000" core="false"/>
    <atomicState n="4" l="0" kappa="1" occ="2.00000" core="false"/>
    <basis>
      <default type="lapw" trialEnergy="0.1500" searchE="false"/>
      <custom l="0" type="lapw" trialEnergy="0.1500" searchE="true"/>
      <lo l="0">
        <wf matchingOrder="0" trialEnergy="1.4200" searchE="true"/>
        <wf matchingOrder="1" trialEnergy="1.4200" searchE="true"/>
      </lo>
      <lo l="0">
        <wf matchingOrder="0" trialEnergy="1.4200" searchE="true"/>
        <wf matchingOrder="0" trialEnergy="-1.62" searchE="true"/>
      </lo>
      <lo l="0">
        <wf matchingOrder="0" trialEnergy="-1.62" searchE="true"/>
        <wf matchingOrder="1" trialEnergy="-1.62" searchE="true"/>
      </lo>
      <lo l="0">
        <wf matchingOrder="0" trialEnergy="-1.62" searchE="true"/>
        <wf matchingOrder="2" trialEnergy="-1.62" searchE="true"/>
      </lo>
      <custom l="1" type="lapw" trialEnergy="-0.72" searchE="true"/>
      <lo l="1">
        <wf matchingOrder="0" trialEnergy="-0.72" searchE="true"/>
        <wf matchingOrder="1" trialEnergy="-0.72" searchE="true"/>
      </lo>
      <lo l="1">
        <wf matchingOrder="1" trialEnergy="-0.72" searchE="true"/>
        <wf matchingOrder="2" trialEnergy="-0.72" searchE="true"/>
      </lo>
      <custom l="2" type="lapw" trialEnergy="0.150000" searchE="true"/>
      <lo l="2">
        <wf matchingOrder="0" trialEnergy="0.3950000" searchE="true"/>
        <wf matchingOrder="1" trialEnergy="0.3950000" searchE="true"/>
      </lo>
      <lo l="2">
        <wf matchingOrder="0" trialEnergy="0.3950000" searchE="true"/>
        <wf matchingOrder="2" trialEnergy="0.3950000" searchE="true"/>
      </lo>
    </basis>
  </sp>
</spdb>
```

B. Convergence tests

In this appendix, we show how the target quantities B_0 and B_0' defined in Section 3.1 depends on the computational parameters **`rgkmax`** and **`ngridk`**, for the case of cubic TiC. Notice that for cubic systems, the three parameters which are specified by **`ngridk`** are identical.

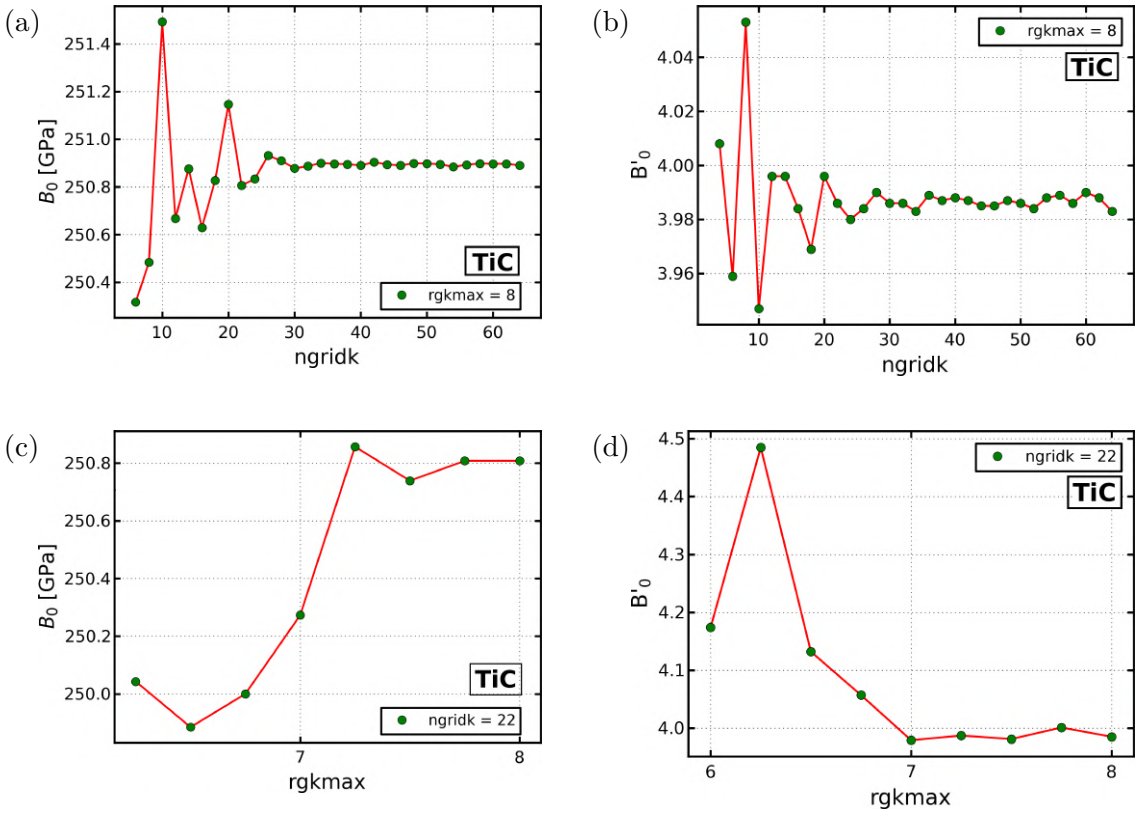

Figure B.1: Convergence test of the target properties, B_0 and B_0', for cubic TiC for the computational parameters **`ngridk`** and **`rgkmax`**.

C. `ElaStic.in` files

This appendix shows the content of the used **`ElaStic.in`** files, which are the input files for the explicit calculation of the second- and third-order elastic constants by the **`ElaStic`** tool. In each file, the first column corresponds to the deformation type, the second gives the maximum strain amplitude $\eta_{\max}$, and the last one the degree of the polynomial used by **`ElaStic`** in the fitting procedure.

TiC, `SOEC` with `PBE`

```
Dst01    0.0700    5
Dst02    0.0700    5
Dst03    0.0475    5
```

TiC, `SOEC` with `PBEsol`

```
Dst01    0.0700    5
Dst02    0.0700    5
Dst03    0.0450    5
```

TiN, `SOEC` with `PBE`

```
Dst01    0.0700    5
Dst02    0.0700    5
Dst03    0.0450    5
```

TiN, `SOEC` with `PBEsol`

```
Dst01    0.0700 5
Dst02    0.0700 5
Dst03    0.0450 5
```

TiC, `TOEC` with `PBE`

```
Dst01    0.0625    5
Dst02    0.0700    5
Dst03    0.0700    5
Dst04    0.0700    5
Dst05    0.0700    3
Dst06    0.0450    5
```

TiC, `TOEC` with `PBEsol`

```
Dst01    0.0625    5
Dst02    0.0625    5
Dst03    0.0700    5
Dst04    0.0700    5
Dst05    0.0700    3
Dst06    0.0450    5
```

TiN, `TOEC` with `PBE`

```
Dst01    0.0700    7
Dst02    0.0700    5
Dst03    0.0400    7
Dst04    0.0700    7
Dst05    0.0700    5
Dst06    0.0700    5
```

TiN, `TOEC` with `PBEsol`

```
Dst01    0.0700    7
Dst02    0.0700    5
Dst03    0.0425    7
Dst04    0.0700    7
Dst05    0.0700    5
Dst06    0.0700    5
```

TiO_2 rutile, `SOEC` with `PBE`

```
Dst01    0.0425    5
Dst02    0.0625    5
Dst03    0.0300    5
Dst04    0.0625    5
Dst05    0.0525    7
Dst06    0.0625    5
```

TiO_2 anatase, `SOEC` with `PBE`

```
Dst01    0.0625    4
Dst02    0.0625    4
Dst03    0.0575    4
Dst04    0.0625    4
Dst05    0.0600    4
Dst06    0.0625    4
```

TiO_2 rutile, TOEC with PBE

```
Dst01     0.125     5
Dst02     0.125     5
Dst03     0.145     5
Dst04     0.105     7
Dst05     0.100     7
Dst06     0.150     5
Dst07     0.125     7
Dst08     0.135     5
Dst09     0.110     5
Dst10     0.110     7
Dst11     0.105     3
Dst12     0.060     5
```

D. TOECs tensor for CI systems

Table D.1: TOECs tensor for cubic CI structures.

$\underline{\underline{\boldsymbol{c}}}^{(3)}_{1jk}$

c_{111}	c_{112}	c_{112}	0	0	0
c_{112}	c_{112}	c_{123}	0	0	0
c_{112}	c_{123}	c_{112}	0	0	0
0	0	0	c_{144}	0	0
0	0	0	0	c_{155}	0
0	0	0	0	0	c_{155}

$\underline{\underline{\boldsymbol{c}}}^{(3)}_{2jk}$

c_{112}	c_{112}	c_{123}	0	0	0
c_{112}	c_{111}	c_{112}	0	0	0
c_{123}	c_{112}	c_{112}	0	0	0
0	0	0	c_{155}	0	0
0	0	0	0	c_{144}	0
0	0	0	0	0	c_{155}

$\underline{\underline{\boldsymbol{c}}}^{(3)}_{3jk}$

c_{112}	c_{123}	c_{112}	0	0	0
c_{123}	c_{112}	c_{112}	0	0	0
c_{112}	c_{112}	c_{111}	0	0	0
0	0	0	c_{155}	0	0
0	0	0	0	c_{155}	0
0	0	0	0	0	c_{144}

$\underline{\underline{\boldsymbol{c}}}^{(3)}_{4jk}$

0	0	0	c_{144}	0	0
0	0	0	c_{155}	0	0
0	0	0	c_{155}	0	0
c_{144}	c_{155}	c_{155}	0	0	0
0	0	0	0	0	c_{456}
0	0	0	0	c_{456}	0

$\underline{\underline{\boldsymbol{c}}}^{(3)}_{5jk}$

0	0	0	0	c_{155}	0
0	0	0	0	c_{144}	0
0	0	0	0	c_{155}	0
0	0	0	0	0	c_{456}
c_{155}	c_{144}	c_{155}	0	0	0
0	0	0	c_{456}	0	0

$\underline{\underline{\boldsymbol{c}}}^{(3)}_{6jk}$

0	0	0	0	0	c_{166}
0	0	0	0	0	c_{166}
0	0	0	0	0	c_{155}
0	0	0	0	c_{456}	0
0	0	0	c_{456}	0	0
c_{155}	c_{144}	c_{155}	0	0	0

Selbstständigkeitserklärung

Ich erkläre hiermit, dass ich die vorliegende Arbeit selbstständig verfasst und noch nicht für andere Prüfungen eingereicht habe. Sämtliche Quellen einschließlich Internetquellen, die unverändert oder abgewandelt wiedergegeben werden, insbesondere Quellen für Texte, Grafiken, Tabellen und Bilder, sind als solche kenntlich gemacht. Mir ist bekannt, dass bei Verstößen gegen diese Grundsätze ein Verfahren wegen Täuschungsversuchs bzw. Täuschung eingeleitet wird.

Berlin, _____